Extended Weak Bonding Interactions in DNA: π-Stacking (Base−Base), Base−Backbone, and Backbone−Backbone Interactions†

Chérif F. Matta, Norberto Castillo, and Russell J. Boyd*

Department of Chemistry, Dalhousie University, Halifax, Nova Scotia, Canada B3H 4J3

Received: September 2, 2005; In Final Form: October 11, 2005

We report on several weak interactions in nucleic acids, which, collectively, can make a nonnegligible contribution to the structure and stability of these molecules. Fragments of DNA were obtained from previously determined accurate experimental geometries and their electron density distributions calculated using density functional theory (DFT). The electron densities were analyzed topologically according to the quantum theory of atoms in molecules (AIM). A web of closed-shell bonding interactions is shown to connect neighboring base pairs in base-pair duplexes and in dinuleotide steps. This bonding underlies the well-known π-stacking interaction between adjacent nucleic acid bases and is characterized topologically for the first time. Two less widely appreciated modes of weak closed-shell interactions in nucleic acids are also described: (i) interactions between atoms in the bases and atoms belonging to the backbone (base−backbone) and (ii) interactions among atoms within the backbone itself (backbone−backbone). These interactions include hydrogen bonding, dihydrogen bonding, hydrogen−hydrogen bonding, and several other weak closed-shell X−Y interactions (X, Y = O, N, C). While each individual interaction is very weak and typically accompanied by perhaps 0.5−3 kcal/mol, the sum total of these interactions is postulated to play a role in stabilizing the structure of nucleic acids. The Watson-and-Crick hydrogen bonding is also characterized in detail at the experimental geometries as a prelude to the discussion of the modes of interactions listed in the title.

1. Introduction

The discovery of the α-helix in the fifties underscored the importance of structural knowledge of the molecules of life in the understanding of biology.[1−7] The local geometry of a segment of a nucleic acid molecule is crucial in determining its properties such as the binding of drugs, mutagens, or proteins, the ease of intercalation by planar foreign molecules, etc. This local geometry is influenced by several weak closed-shell interactions. These weak interactions include, for example, the Watson−Crick (WC) hydrogen bonding within a base pair and the stacking interactions in stacked base duplexes.[8−11] WC base pairing is the glue holding the two complementary strands of DNA together. The puckering of the sugar moiety determines the type of DNA (A, B, or Z) which, together with the base stacking interaction, determine such helical geometrical properties as the helix pitch, the number of residues per turn, the axial rise (the spacing between base pair stacks), the helix diameter, etc.

In this paper, we provide insight into the closed-shell bonding interactions driving the intramolecular recognition in DNA responsible for its local geometry. While much literature exists about the geometry and energy of π-stacking interactions, no previous reports discuss the electron density characteristics underlying π-stacking in nucleic acids, to the best of our knowledge. In this paper, the importance of the noncovalent interactions between the nucleobases and the backbone and within the backbone itself is emphasized.

The present study characterizes the π-stacking interactions between nearest neighbor stacked bases, the interactions that a given nucleobase has with the backbone, and the interactions within the backbone itself. The characterization of the bonding is based on the topology of the electron density distribution[12] accurately calculated from density functional theory (DFT) using the experimental geometries of real segments of DNA.

This study is not meant to be comprehensive, rather, a sample of only four dimer duplexes out of the 16 possibilities is scrutinized. Further, we chose B-DNA since it is the most abundant form of DNA and since it has an intermediary step height falling between the more compact A-DNA and the more expanded Z-DNA.

The paper is organized as follows. To set the context of this work, recent literature is discussed in two sections, one dealing with π-stacking and the second with base−backbone interactions. The Results and Discussion section is organized to reflect these two modes of interactions. Since frequent reference is made to individual bonding interactions, the numbering scheme of the nucleobases (Figure 10) and of the backbone (Figure 11) is given in the Appendix.

2. π-Stacking of Neighboring Nucleobases in a Dinucleotide Step

Aromatic π-stacking is of paramount importance in regulating some mechanisms at the gene level. For example, the enzyme−nucleic acids recognition regulating gene expression is largely controlled by π-stacking of aromatic amino acids and nucleobases.[13,14] Furthermore, neighboring base-pair stacking controls the gross geometrical feature of a nucleic acid macromolecule.[15,16] Local nucleotide sequences determine a nucleic acid's stiffness and the propensity of a segment to fold, kink, or supercoil and is, therefore, responsible for creating the local

* To whom correspondence should be addressed. E-mail: russell.boyd@dal.ca. Tel: (902) 494-8883. Fax: (902) 494-1310.

† Abbreviations and definition of the terminology used in this paper are provided in the Appendix.

10.1021/jp054986g CCC: $33.50
Published on Web 12/09/2005

geometry needed for proper enzymatic recognition.[17] The ease of intercalation of a planar molecule between two stacked nucleic acid base pairs is negatively correlated with the strength of their π-stacking.[9] The recent ground-breaking work by Meggers et al.[18] has established that DNA polymer analogues which completely lack the backbone sugar residues retain the capability of forming the characteristic α-double helix, with stacked base pairs in the usual Watson−Crick base-pairing scheme.[18] While hydrogen bonding plays a major role in gluing the two intertwined helices together, we conjecture that the π-stacking interaction is perhaps as important in preserving the α-helical structure despite the absence of sugar residues. Recent evidence suggests that the interstrand hydrogen bonding and the nearest neighbor base π-stacking interaction are not independent, as the stacking of nucleobases influences their hydrogen bonding capacity.[19]

A voluminous literature reports the energetics of π-stacked monomer duplexes (dinucleobases) and WC dimer duplexes (dinucleobase dimers) (see, for example, refs 20−24 and references therein). Since the stacking of nucleic acid bases is due to weak closed-shell interactions, the determination of such energies necessitates an explicit treatment of electron correlation, such as MP*n* or CI.[20−22] Furthermore, evidence suggests that stacking energy is highly sensitive to the quality of the basis set, which should be augmented with special diffuse polarization functions.[25] None of the popular DFT functionals was able to reproduce the energetic trends and equilibrium geometries calculated at the MP2 level even for the simplest test case of the different benzene dimers.[26] Zhao and Truhlar are developing a new DFT-based extrapolation scheme that promises to provide accurate estimates of π-stacking energies.[27,28] At present, however, one is only left with prohibitively expensive options to calculate base-pair stacking energies of nucleobases from a proper post-Hartree−Fock method.

Recently, Zhikol et al.[29] described an electron density-based parametrization which reproduces the benzene dimer potential energy surface using the DFT hybrid functional B3LYP. These authors used AIM[12] to study the topology of the electron density between the planes of the two interacting benzene monomers. (The AIM theory has been reviewed elsewhere by its principal author[12,30−33] and, at an introductory level, by others.)[34,35] Zhikol et al. studied 10 π-stacking geometries of the benzene dimer, and in each case, they found bond path(s) (defined in ref. 36) linking the monomers. The number of bond paths linking the two monomers ranges from 12 (the staggered conformation) to only one depending on the orientation of the two ring planes. Interestingly, even in the cases where only one bond path links the two rings, a cage critical point (CCP) was found between the two rings.[29] The latter observation is the first realization of this mathematical possibility in a molecular complex in the absence of a cage of bond paths (the first observation of such a CCP in a single ring within a molecule has been recently reported).[37] Zhikol et al. obtained an empirical relation between the binding energy calculated at the MP2(full)/6-31+G(2d,2p) level—with slightly more diffuse d-functions than in the standard Pople basis set—and properties of the electron density at the CCP ($r = 0.9972$). The entire potential energy curve representing the π-stacking energy could be reproduced by these workers using the properties of the electron density sampled at the CCP. Their fitting included the electron density at the CCP and terms depending on the Laplacian and its square to correct for the monotonic decrease of the density with the distance of separation of the two monomers.[29]

3. Nucleobase−Backbone Closed-Shell Bonding Interactions

A nucleobase can be oriented syn or anti with respect to the sugar moiety, with a rather restricted rotation of the base with respect to the sugar. Hydrogen bonding between the nucleobase (or a derivatized nucleobase) and atoms in the backbone can influence the relative syn/anti stability and contribute to the prevalence of one conformation over the other.[9] The free hydroxyl (O5′H) in a *free* nucleotide can hydrogen bond with N3 of the purine base or (O2 of the pyrimidine base).[9]

Nuclear Overhauser effect (NOE) studies of A- and B-DNA have revealed the presence of short proton−proton distances connecting the base H8 or H6 to the sugars H1′, H2′a, and H2′b which in turn exhibit similar short contacts with the next base, and so on. This connectivity pattern, which runs in each of the two strands in the 5′ → 3′ direction, has been termed "sequential connectivities".[38−40]

An early NMR study suggests that derivatization of the bases in nucleotides (e.g., 8-NH_2-AMP, 8-$NH(CH_3)$-AMP, and 8-$N(CH_3)_2$-AMP) can change the base's conformation from the preferred syn to the anti.[41] The authors of this study attribute this conformational change to electrostatic repulsion between the backbone's electron-rich phosphate and O1′ and O5′ of the ribose sugar with the base's substituent at position 8. In addition, the authors propose that the anti conformation is further stabilized by a hydrogen bond between the 8-amino hydrogen (present only in the primary and secondary amines) and O5′. While the bases in these experiments are derivatized, the work highlights the influence of the backbone−base interaction on the geometry of the nucleotide.

Thus, experimental evidence suggests a nonnegligible base−backbone closed-shell interaction, at least hydrogen bonding between the sugar and the proximal base protons. Hocket and co-workers have recently shown the role of several stabilizing hydrogen bonding interactions between the backbone and the base in all single 2′-deoxyribo-[42,43] and ribonucleosides.[44] Hocket et al. charaterized these interactions on the basis of the topology of the electron density according to the AIM theory.

Further, two recent reports[45,46] provide new insight into carbohydrate−protein molecular recognition, an interaction largely mediated by hydrogen bonding.[46] In their paper, Fernández-Alonso et al. study the energetic and electron density changes along the potential energy surface of association of a benzene molecule (representing an aromatic amino acid residue) and a fucose molecule (representing a typical sugar found in the biological milieu). They provide NMR and theoretical evidence of the existence of stabilizing carbohydrate−aromatic interactions with an important dispersive component.[46] The AIM topological study as well as the NMR evidence shows that there exist several nonconventional hydrogen bonded interactions in the sugar−benzene complex with a net stabilization energy of 3.0 kcal/mol (a value obtained after BSSE correction by the counterpoise method at the MP2/6-31G(d,p) level). The results of Fernández-Alonso et al.[46] suggest that similar interactions are likely to be taking place between the nucleobases and the neighboring sugar within a nucleotide or between sugar residues belonging to neighboring nucleotides. Evidence for the existence of such bonding is presented in this paper, bonding that can contribute to the structure and stability of DNA through additivity and cooperativity.

4. Method

We performed single-point calculations on DNA fragments extracted from a decamer $d(CATGGCCATG)_2$, the geometry

of which was determined by high-resolution NMR spectroscopy.[47] We have also used the middle portion (denoted by parentheses) of the high-resolution (1.4 Å) X-ray crystallographic structure[48,49] of the dodecamer CGCG(AATT)CGCG. The coordinates of the portion of interest were extracted from the Protein Data Bank (PDB) file after the removal of all solvent molecules. The models were then completed by saturating all dangling bonds with hydrogen atoms placed at standard positions. A single-point density functional calculation was then performed on each model frozen at the experimental geometry. All electronic structure calculations were performed at the B3LYP/6-311++G(d,p) level. The Gaussian 03[50] package was used in the electronic structure calculations. The resulting electron densities were analyzed according to the quantum theory of atoms in molecules[12] using the AIM 2000[51] program, which was also used to generate the molecular graphs.

5. Results and Discussion

There are 16 possible WC duplexes of dimers that occur in DNA, and since there are at least three major types of DNA (A, B, and Z), a complete investigation of the closed-shell bonding interactions would require the consideration of at least 48 duplexes. Such a study would be prohibitive with regards to the presently available computational and human resources. Since B-DNA is the most common DNA, we chose this form in the present work and considered in detail a sampling of four dimer duplexes out of the 16 possibilities. Similar bonding interactions were found to recur in the four dimer duplexes we have studied, and it is expected that similar bonding occurs in the remaining dimer duplexes that were not included in this study.

If the backbone is included for a study of base−backbone interactions, one can have 16 possible monomer duplexes in a dinucleotide (when the nonequivalence of the 5′ → 3′ and 3′ → 5′ directions is taken into account). Thus, again, we sampled the base−backbone space by considering four representatives out of the 16 possible dinucleotides. The model for the dinucleotides was simplified by replacing the phosphate group of the second nucleotide with a hydrogen atom at the 3′b position. Furthermore, we have also replaced the 5′ group [−C(5′)H_2O(5′)−] of the first nucleotide with a hydrogen atom. Thus, the model referred to in this paper as "dinucleotide" consists, strictly, of a 5′-pseudo-nucleotide-3′-nucleoside sequence.

This paper presents a characterization of the bonding in these model systems based on the properties of the bond paths traced in the respective electron density distributions. A bond path is defined according to the AIM theory as a line of maximum electron density in real three-dimensional space linking chemically bonded nuclei when the system is in an equilibrium geometry.[36] Similar lines found in systems which are not at equilibrium are termed *atomic interaction lines*. The systems studied here are extracted from experimental geometries which must exist, in nature, at equilibrium. Thus, in this paper, we will refer to all atomic interaction lines as "bond paths".

In Figures 1−8, two representations are shown for the molecular graph, that is, the collection of bond paths defining the molecular structure. In each figure, part **a** provides a view of the actual tracings of the bond paths along with the location of the critical points (CPs) [bond (BCPs), ring (RCPs), and cage critical points (CCPs)]. Part **b** provides a simplified version of the molecular graph showing only the connectivities in the familiar ball-and-stick representation. Thus, part **b** does not show the curvature of bond paths as in part **a**. Each figure is then followed by a corresponding table, of the same number as the figure, which lists the principal bond properties of the weak interactions, each labeled with reference to the two atoms involved in the bonding. The atomic numbering follows accepted conventions supplemented with additional labeling for the hydrogen atoms (Appendix, Figures 10 and 11).

5.1. Nucleobase Dimer Duplexes. The nucleobase dimer duplexes considered in this study are

$$\downarrow\left|\begin{matrix}\mathbf{A5-T8}\\ \mathbf{A6-T7}\end{matrix}\right|\uparrow \text{ (Table and Figure 1),}$$

$$\downarrow\left|\begin{matrix}\mathbf{T8-A5}\\ \mathbf{C9-G4}\end{matrix}\right|\uparrow \text{ (Table and Figure 2),}$$

$$\downarrow\left|\begin{matrix}\mathbf{G4-C7}\\ \mathbf{G5-C6}\end{matrix}\right|\uparrow \text{ (Table and Figure 3),}$$

$$\text{and}\downarrow\left|\begin{matrix}\mathbf{G5-C6}\\ \mathbf{C6-G5}\end{matrix}\right|\uparrow \text{ (Table and Figure 4),}$$

where the numbers indicate the position of the base in the DNA sequence in the experimental DNA α-helix from which it was extracted and the arrows point in the 5′ → 3′ direction. For simplicity, the following more compact notations will also be used to denote the above dimer duplexes: A5T8/A6T7, T8A5/C9G4, G4C7/G5C6, and G5C6/C6G5, respectively. In the following section, the bonding in WC dimers will be examined first and then the focus will be shifted to the π-stacking interactions.

5.1.1. Watson-Crick Hydrogen Bonding. The textbook depiction of the WC DNA base pairs assigns two hydrogen bonds to the AT (or AU) pair and three to the GC pair. This traditional depiction of the AT doubly hydrogen bonded WC dimer leaves O2 of the pyrimidine base as an unfulfilled hydrogen bond acceptor on the minor-groove side. Crick himself remarked as early as 1966 that this may induce instability in the architecture of DNA.[52] Leonard et al.[53] provided arguments in favor of a third hydrogen bond in the AT pair and anticipated ∼1 kcal/mol of stabilization due to this bonding based on geometric arguments.

Recently, Parthasarathi and co-workers performed a comprehensive study of the hydrogen bonding in several types of nucleic acid base pairs, including the WC pairing scheme.[54] These authors report, for the first time, the molecular graph of the AT pair exhibiting a bond path linking A(H2) and T(O2) along with a tabulation of its topological properties. A year earlier, Asensio et al.[55] provided energetic estimates of each of the hydrogen bonding interactions in WC dimers separately at the counterpoise BSSE-corrected MP2/D95(d,p) level. In their study, Asensio et al. also considered the energy of this third weak hydrogen bond in the AT dimer, AT-III. They estimated the energy of the individual hydrogen bonds in the WC dimers from the binding of dimers which are constrained by rotating the plane of one of the bases so that it becomes perpendicular to the plane of the other, with the two planes intersecting approximately at the axis of the hydrogen bond in question. This procedure eliminates a large fraction of the cooperativity occurring in such triply hydrogen bonded systems, the cooperativity being defined as the difference between the dimer binding and the sum of the individual H-bond energies. The cooperativity was found to be ∼3 kcal/mol for each of the two dimers, AT and GC.[55]

There exist strong relationships between the topological bond properties and the bond energy (E) defined as the negative of bond dissociation energy ($E = -D_e$), if one disregards ZPE

and temperature corrections. For instance, the electron density at the bond critical point has been shown on numerous occasions to be strongly correlated with the bond dissociation energy for a variety hydrogen bonds, a separate regression being necessary for each class of hydrogen bond (see, for example, refs 56−62). A study of 83 hydrogen bonds of the type X−H···O (X = C, N, O) revealed strong exponential correlations, on one hand, between D_e and the bond distance d(H···O) and, on the other hand, between the potential energy density (the virial field strength) at the BCP (V_b) and d(H···O).[58] Since the exponents in both correlations were found to be almost identical (∼3.6), this suggested a proportionality between the X−H···O hydrogen bond energy and the virial field strength evaluated at the BCP, V_b.[58] The empirical fit yielded the following approximate relation which we will call the Espinosa, Molins, and Lecomte relation (EML)[58]

$$E = kV_b \tag{1}$$

where k is a proportionality constant having the dimensions of volume ($k \approx 0.5$ au for the X−H···O hydrogen bond).

Further, Espinosa and Molins (EM)[63] obtained an interaction potential from the AIM analysis of the same data set of 83 X−H···O hydrogen bonds.[58] EM have shown that the interaction potential is proportional to the total energy evaluated at the H···O BCP. The EM potential closely reproduces Morse- and Buckingham-type potentials provided that the well depth (U_0) and position (r_0) as well as the curvature of the potential at r_0 are constrained to assume the same values in each potential.[63]

The above EML empirical relationship between E (or D_e) and V_b is remarkable and very useful because it allows one to estimate a global property such as the bond dissociation energy solely from the knowledge of the potential energy density at a single point, the BCP. Thus, D_e can be estimated from V_b determined at the true equilibrium geometry of the system. If one has a regression equation relating the D_e to V_b for each one of the three different types of WC hydrogen bonds, namely, N−H···N, N−H···O, and C−H···O, then one could estimate the contribution each bond is making to the binding of the WC dimer. (Work is in progress in our lab to obtain these regressions. In this paper, preliminary estimates are presented on the basis of the EML regression for the X−H···O bonds.) The EML approach obviates the need to artificially rotate the plane of one base 90° with respect to the other to estimate the energy of the sought-after interaction in a WC dimer as in the work by Asensio et al.[55] described above. A second advantage is that there would be no need, in principle, to consider cooperativity explicitly, since it should be factored in within the bond properties determined at the BCP. The limitation of eq 1 is that each type of hydrogen bond requires a separate regression carefully designed to bracket the interaction of interest, each regression yielding a different k, and all data must be collected at one and the same level of theory (unlike the EML data set).

The average properties for the WC hydrogen bonding along with the estimated bond energies obtained from Asensio et al.[55] as well as those estimated via EML eq 1 are listed in Table 9.

From Table 9, one can distinguish three types of WC hydrogen bonds: N−H···O [AT-I, GC-I, GC-III], C−H···O [AT-III)], and N−H···N [AT-II, GC-II]. The common properties shared by all the hydrogen bonds in the two WC base pairs are discussed first followed by a discussion of the characteristics of each class separately.

Common Characteristics of the Six Watson−Crick Hydrogen Bonding Interactions. None of the WC bonding interactions exhibit a significant deviation of the bond path from linearity, as can be seen in Table 9 from the differences between the bpl's) and the bl's. The largest of these deviations is only 0.047 Å in the case of the weakest interaction (AT-III). The values of ρ_b fall in the range 0.052−0.006 au, which outflank the range of common hydrogen bonds (strong hydrogen bonds as in H_3N···HF ($\rho_b = 0.034$ au), intermediate as in HF···HF ($\rho_b = 0.021$ au), and weak as in HCl···HF ($\rho_b = 0.007$ au)).[57] The Laplacian, $\nabla^2\rho_b$, assumes positive values for all six bonds as expected for closed-shell interactions. For each one of the six bonds, none exhibit a marked ellipticity (ϵ), since the magnitude of the dominant negative curvature ($\lambda 1$) is not much larger than the magnitude of the soft negative curvature ($\lambda 2$) in each case.

Watson−Crick X−H···O (X = N, C) Hydrogen Bonding. The average experimentally estimated H···O separations in the two N−H···O hydrogen bonds of the GC base pair (1.87 and 1.90 Å, for I and III, respectively) are both significantly shorter than the corresponding bond in AT (2.12Å). This is accompanied by much less accumulation of electron density in the latter's BCP ($\rho_b \sim 0.02$ au) compared to that ($\rho_b \sim 0.03$) in the two N−H···O belonging to GC (Table 9). The H···O separation is significantly longer in the case of the weak and recently characterized third hydrogen bond in AT (AT-III), reaching a length of 2.79 Å with a ρ_b value of only 0.006 au. Further, from Table 9, the curvature along the bond path ($\lambda 3$) is also softer in AT-I (and much more so for AT-III) than in GC-I, and GC-III, again indicative of less accumulation of density at the BCP along the bond path. The two negative curvatures ($\lambda 1$ and $\lambda 2$) which are perpendicular to the bond path assume, in the case of AT-I, less than half of their magnitude in GC-I or GC-II. And since the magnitude of $\lambda 1$ is not much greater than $\lambda 2$ in each of the four bonds, the resulting ellipticities (ϵ) are negligible.

The virial field $V(\mathbf{r})$ is negative everywhere in a molecule; in contrast, the kinetic energy density $G(\mathbf{r})$ is positive everywhere. The local expression of the virial theorem for a system in electrostatic equilibrium, relating these two quantities at the BCP, is written[12,64]

$$V_b = \left(\frac{\hbar^2}{4m}\right)\nabla^2\rho_b - 2G_b \tag{2}$$

In a shared bonding interaction, V_b dominates (i.e., $|V_b| > |2G_b|$ or, equivalently, $\nabla^2\rho_b$ is a negative quantity) and electrons are accumulated at the BCP. The situation is reversed in closed-shell bonding, and in this case, $\nabla^2\rho_b$ is positive. The borderline between a shared and a closed-shell interaction is thus when $\nabla^2\rho_b = 0$. Since energy densities have the dimensions of pressure (force per unit area), Espinosa et al.[58] proposed the interpretation of the potential energy density at the BCP, V_b, as the pressure exerted by the system on the electrons which tends to concentrate them at this point. On the other hand, the kinetic energy density at the BCP, G_b, was interpreted as the pressure exerted by the electrons at that point on the system (the reaction to V_b), which tends to "dilute" the electrons away from that point.[58] As can be seen from Table 9, the magnitudes of both G_b and V_b in the case of AT-I are again less than half of the corresponding magnitudes for GC-I and GC-III.

Finally, Cremer and Kraka[65] suggested the use of the electronic energy density evaluated at the BCP

$$H_b = G_b + V_b \tag{3}$$

to compare the kinetic and potential energies on an equal footing (instead of the 2:1 ratio in the local expression of the virial

theorem (eq 2)). Generally, H_b assumes negative values for interactions with significant sharing of electrons; its magnitude reflects the "covalent character" of the bonding.[65] No particular trends can be gleaned from Table 9 from the values of H_b in these four bonds, except that they assume negative values for the N−H···N hydrogen bonds as discussed below.

The last column in Table 9 lists the estimates of the individual hydrogen bond energies (in kcal/mol) obtained by the procedure of Asensio et al.[55] (vide supra). While Asensio et al. also report estimates of these energies at four theoretical levels, including MP2/D95(d,p), we list the values obtained from the closest level of theory used by these authors to our own, that is, B3LYP/D95 without BSSE correction, for a valid comparison. In Table 9, we also list our estimates of the individual bond energies in the DNA base pairs obtained using the EML approximation.[58] Energies of the X−H···O interactions were estimated directly from the EML equation (eq 1), but energies of the N−H···N interactions were calculated by the difference. To obtain more accurate estimates, we relied on V_b values calculated using densities obtained at the B3LYP/6-311++G(d,p) level but with geometries fully optimized at the B3LYP/6-31+G(d,p) level and to be published elsewhere.[66] Our individual bond energy estimates for the four X−H···O bonds differ from those obtained by Asensio et al. In the GC pair, for example, we find that the bond energy of GC-I is larger than that of GC-III, which is also reflected in the values of ρ_b, a result opposite to the Asensio et al. findings: E(GC-I) = 10.5 (5.4) kcal/mol and E(GC-III) = 6.3 (12.5) kcal/mol (values in parentheses are those of Asensio et al.). This discrepancy might in part arise from the artificial restriction of the planes of the two bases to be perpendicular to one another in the work of Asensio et al. and partly due to the drastic approximations assumed in deriving eq 2 and in the limitations of the data set used by EML in the statistical fitting. Both our estimate and Arsenio's estimate, however, agree on the magnitudes of AT-I (∼6 kcal/mol) and AT-III (∼1 kcal/mol), an agreement which may be coincidental or due to a cancellation of errors. A source of error in our calculation is the fact that eq 1 (with $k = 0.5$ au) was obtained by analyzing a data set consisting of 83 X−H···O hydrogen bonds computed at several different ab initio levels of theory, none being the one used in the present study. Our estimates are therefore at best taken as indicative of relative trends rather than absolute bond energies.

Watson−Crick N−H···N Hydrogen Bonding. This bond is significantly shorter in AT [d(H···N) ≈ 1.73 Å] than in GC [d(H···N) ≈ 1.85 Å], with a consequent larger accumulation of density at the BCP of the former ($\rho_b = 0.052$ au) than at the latter ($\rho_b = 0.038$ au). Both bond paths do not deviate significantly from linearity (small bpl−bl differences). Both bonds exhibit the hallmark of closed-shell bonding (positive values of $\nabla^2\rho_b$) but exhibit a negative total energy density at the BCP (H_b) which—while not impossible—is uncommon for closed-shell interactions and indicate a degree of electron sharing.

The average bond properties for the WC N−H···N (Table 9) are remarkably close to those calculated for this bond in small model molecular complexes exhibiting similar internuclear separation despite that they were calculated at a different level of theory (restricted Hartree−Fock (HF) theory 6-31G(d,p)).[67] Thus, the properties of the N−H···N bond in complex **21** $[H_3NH\cdots NH_3]^+$ reported in ref 67 with d(H···N) = 1.728 Å are to be compared to the average AT-II bond (d(H···N) = 1.725 Å) properties listed in Table 9 (and given here in parentheses); all values are rounded to the third decimal and given in atomic units: $\rho_b = 0.051$ (0.052), $\nabla^2\rho_b = 0.108$ (0.093), $\lambda 12$ (average of the two negative curvatures $\lambda 1$ and $\lambda 2$) = −0.085 (−0.089), $\lambda 3 = 0.278$ (0.271), and $G_b = 0.032$ (0.034). On the other hand, the longer N−H···N bond in GC-II should be compared with complex **29** $[LiCNH\cdots NCF]^+$ or **31** $[FH_2NH\cdots NCCN]^+$ reported in ref 67 both of which exhibit the same d(H···N) = 1.850 Å which is the closest value to the GC-II bond length (1.854 Å) in Table 9. The bond properties for this bond in **29** and **31** are very similar; we average them here (in parentheses) and comparing with GC-II we have (all values in au): $\rho_b = 0.030$ (0.038), $\nabla^2\rho_b = 0.099$ (0.100), $\lambda 12 = -0.044$ (−0.057), $\lambda 3 = 0.187$ (0.215), and $G_b = 0.022$ (0.028). This comparison is indeed remarkable in view of the different theoretical method, different basis sets, and even slightly different bond lengths and different complexes being included in the comparison and shows how relatively method-independent AIM properties are.

Since a fit similar to eq 1 for the N−H···N hydrogen bond is not in our possession at present, it is not possible to estimate its bond energy directly as we did in the case of the X−H···O bond. However, we may obtain an estimate by difference, since the total binding between the two monomers is known for the base pairs (entries in the rows labeled AT and GC in Table 9) and the energies of the other interactions (X−H···O) were obtained directly from the EML equation. This estimate, however, is to be taken cautiously in view of error propagation and in view of the systematic errors in the estimates of the energies of the X−H···O due to the inconsistency of the level of theory.

It is surprising that N−H···N bond energies calculated in this manner are close to the estimates of Asensio et al.,[55] E(AT-II) = 5.8 (4.8) kcal/mol and E(GC-II) = 8.9 (8.8) kcal/mol (values in parentheses are those of Asensio et al.). It is also surprising that the AT-II bond, which is 0.129 Å shorter than GC-II and as a result exhibits a significantly higher ρ_b ($\rho_b = 0.041$ au for AT-II vs $\rho_b = 0.033$ au in the case of GC-II), is the one estimated to have the lower hydrogen bond energy of the two. It is believed that this apparent discrepancy could be an artifact of overestimating the X−H···O hydrogen bond energies leaving little energy recovered by difference from the total dimer binding energy.

A study is underway in our laboratory to calibrate E vs V_b (and other bond properties) relationship(s) for each type of hydrogen bond occurring in WC dimers at a consistent level of theory. This could allow the direct estimation of the contribution of each WC hydrogen bond to the total binding at the equilibrium geometry without the need to artificially rotate the base pairs in planes perpendicular to one another.

5.1.2. π-Stacking in a Dinucleotide Duplex. The stacking interactions are subdivided into *intra*strand and *inter*strand. These two types of interactions can be symbolized by the double-headed arrows in

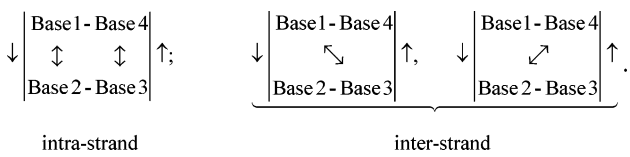

A bond path linking atoms in stacked bases belonging to one and the same strand of the double helix will be termed an *intrastrand interaction* and one that links an atom in a base belonging to one strand to another in a stacked base belonging to the opposite strand will be referred to as an *interstrand interaction*. In this section, the complex web of bond paths

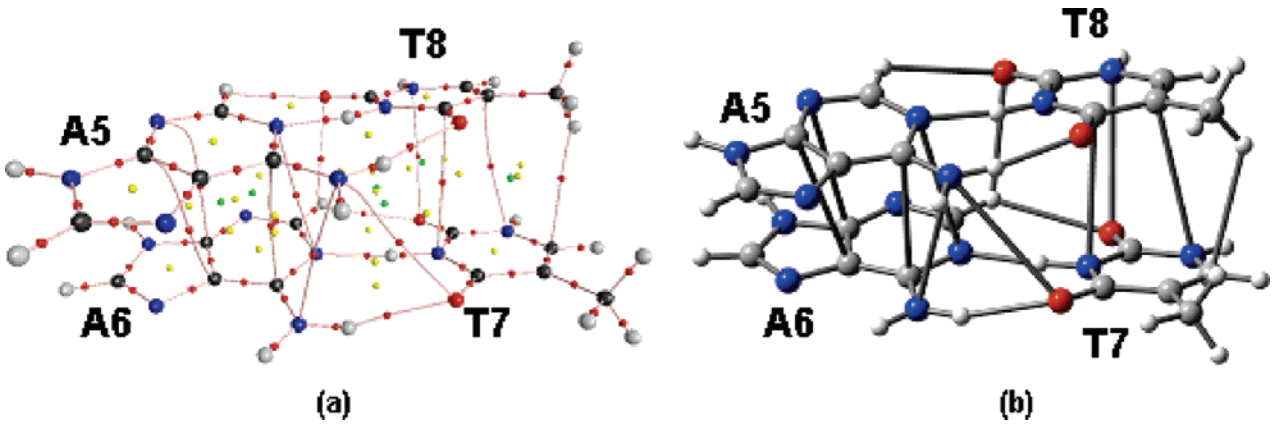

Figure 1. (a) Molecular graph of an AT/AT duplex of Watson−Crick dimers. The base numbering refers to the placement of the base in the experimental structure[48,49] from which the model has been taken. The large spheres represent the nuclei of atoms: black = C, red = O, blue = N, and gray = H. The lines connecting the nuclei are the bond paths traced within the electron density distribution. The small dots indicate the positions of the critical points (stationary points in the density): red = bond critical points (BCP), yellow = ring critical points (RCP), and green = cage critical points (CCP). The bond properties corresponding to this molecular graph are listed in Table 1. (b) A simplified ball-and-stick representation of the molecular graph where bond paths located in the electron density are represented by sticks. The color coding in part **a** of this caption also applies to Figures 2−9.

TABLE 1: Closed-shell Bonding in the $\downarrow\left|\begin{matrix}\text{A5−T8}\\ \text{A6−T7}\end{matrix}\right|\uparrow$ Dimer Duplex[a]

bases[b]	bond[b]	bl	bpl	bpl−bl	ρ_b	$\nabla^2\rho_b$	$\lambda1$	$\lambda2$	$\lambda3$	ϵ	G_b	V_b	H_b
Watson−Crick H-bonding													
A5−T8	H6a−O1	2.011	2.034	0.024	0.022	0.077	−0.029	−0.028	0.133	0.047	0.017	−0.015	0.002
A5−T8	N1−H3	1.749	1.767	0.018	0.049	0.093	−0.084	−0.080	0.257	0.056	0.032	−0.042	−0.009
A5−T8	H2−O2	2.874	2.930	0.057	0.005	0.016	−0.004	−0.003	0.023	0.150	0.003	−0.003	0.001
A6−T7	H6a−O1	2.213	2.239	0.026	0.014	0.047	−0.016	−0.015	0.078	0.049	0.010	−0.008	0.002
A6−T7	N1−H3	1.738	1.757	0.019	0.050	0.093	−0.087	−0.082	0.262	0.056	0.033	−0.043	−0.010
A6−T7	H2−O2	2.657	2.699	0.042	0.007	0.023	−0.006	−0.006	0.034	0.082	0.005	−0.004	0.001
Stacking (intrastrand)													
A5−A6	N6−N6	3.368	3.374	0.006	0.006	0.016	−0.004	−0.003	0.023	0.574	0.004	−0.003	0.000
A−-A6	C6−C6	3.332	3.352	0.020	0.005	0.018	−0.001	−0.000	0.020	4.537	0.004	−0.003	0.001
A5−A6	N1−N1	3.397	3.402	0.005	0.005	0.016	−0.003	−0.002	0.020	0.875	0.003	−0.003	0.000
A5−A6	N3−C4	3.508	3.816	0.308	0.005	0.014	−0.002	−0.001	0.017	0.928	0.003	−0.002	0.001
A5−A6	C4−C5	3.559	3.895	0.335	0.005	0.014	−0.002	−0.000	0.016	2.682	0.003	−0.002	0.001
T7−T8	N1−O2	3.476	3.478	0.002	0.004	0.013	−0.002	−0.002	0.017	0.311	0.003	−0.002	0.000
T7−T8	C5−N1	3.573	3.650	0.077	0.005	0.012	−0.002	−0.001	0.016	0.522	0.003	−0.002	0.000
T7−T8	C6−H5b	2.878	2.920	0.042	0.005	0.016	−0.003	−0.002	0.022	0.290	0.003	−0.003	0.001
T7−T8	C4−N3	3.389	3.417	0.028	0.005	0.016	−0.003	−0.001	0.020	1.336	0.003	−0.003	0.001
Stacking (interstrand)													
A5−T7	N6−O1	3.613	3.645	0.032	0.003	0.010	−0.002	−0.001	0.013	0.606	0.002	−0.002	0.001
A6−T8	H2−O2	2.741	2.851	0.110	0.006	0.022	−0.005	−0.004	0.030	0.306	0.005	−0.004	0.001

[a] The electron density was calculated at the B3LYP/6-311++G(d,p) level at the experimental geometry obtained from refs 48 and 49. All entries are in atomic units (au) except bond lengths (bl's) and bond path lengths (bpl's) and their differences which are in angstroms. [b] Labeling convention: The column labeled "bond" lists the two atoms involved in the bonding, the first atom belonging to the first base listed under "bases" and the second belonging to the second base. Thus, the first entry (A5−T8, H6a−O1) means that the bonding is between atom H6a belonging to the base A5 and atom O1 belonging to base T8. Atom numbering schemes of the bases and the backbone are given in Figures 10 and 11, respectively, of the appendix. The same conventions are adopted in Tables 2−4.

linking each of the four dimer duplexes considered in this paper will be discussed separately.

From the previous discussion of the WC hydrogen bonding (and Table 9), a hydrogen bond such as AT-III characterized by $\rho_b \approx 0.006$ can be associated with a bond energy of perhaps ~1 kcal/mol. While, in isolation, such a bond contributes a relatively minor stabilizing energy, the cumulative effect of several such weak bonding interactions between π-stacked bases may not be negligible. With this in mind, very weak π-stacking interactions will be discussed only briefly and collectively reserving more detailed examination to those interactions with $\rho_b > 0.01$ au.

Table 10 lists the average bond properties over *n* representatives of each class of weak closed-shell bonding interactions found in this study, at the exclusion of the WC hydrogen bonding already discussed above. The averaging in Table 10 includes all modes of weak bonding interaction found in this study other than the WC hydrogen bonding, namely: π-stacking interactions (inter- and intrastrand), base−backbone, and backbone−backbone interactions.

All the interactions in Table 10 are clearly of the closed-shell type exhibiting positive values of both the Laplacian $\nabla^2\rho_b$ and the total energy density H_b. From the table, one finds that several hydrogen bonding interactions occur in DNA, the X−H···O interaction being the most frequent in the studied DNA fragments (26 bonds). The interactions listed in Table 10 are extremely weak except X−H···O hydrogen bonding which is characterized by $\rho_b = 0.017 \pm 0.012$ au. On the basis of the EML phenomenological approximation,[58] eq 1, the average X−H···O bond energy can be of the order of 4 kcal/mol.

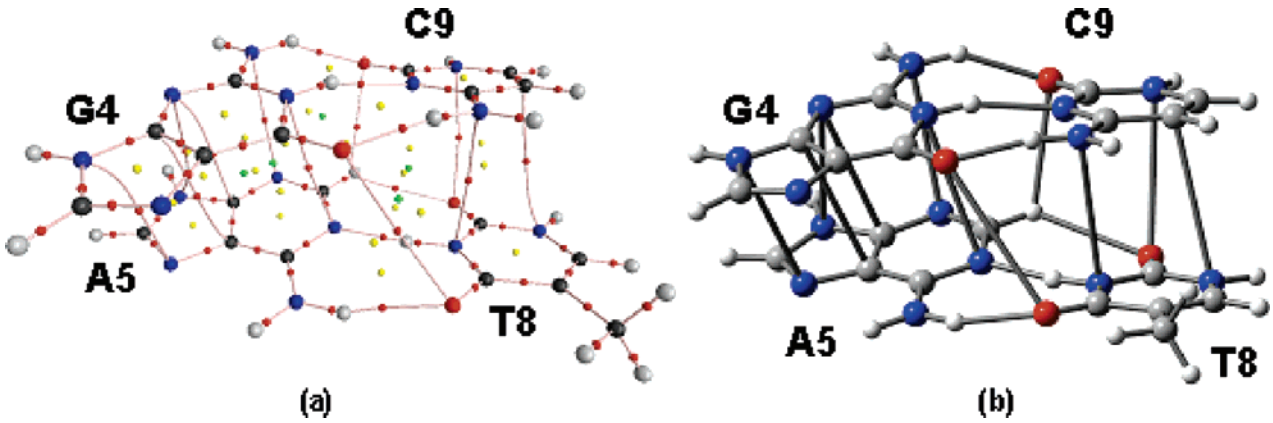

Figure 2. (a) Molecular graph of a GC/AT duplex of Watson−Crick dimers. The base numbering refers to the placement of the base in the experimental structure[48,49] from which the model has been taken. See the caption of Figure 1 for the color coding. The bond properties corresponding to this molecular graph are listed in Table 2. (b) A simplified ball-and-stick representation of the molecular graph where bond paths located in the electron density are represented by sticks.

TABLE 2: Closed-Shell Bonding in the $\downarrow\left|\begin{matrix}\text{T8}-\text{A5}\\ \text{C9}-\text{G4}\end{matrix}\right|\uparrow$ Dimer Duplex[a]

bases[b]	bond[b]	bl	bpl	bpl−bl	ρ_b	$\nabla^2\rho_b$	$\lambda1$	$\lambda2$	$\lambda3$	ϵ	G_b	V_b	H_b
						Watson−Crick H-bonding							
G4−C9	H2a−O2	1.983	2.011	0.028	0.023	0.086	−0.031	−0.029	0.146	0.087	0.019	−0.017	0.002
G4−C9	H1−N3	1.943	1.965	0.022	0.031	0.091	−0.045	−0.042	0.177	0.078	0.023	−0.022	0.000
G4−C9	O6−H4a	1.841	1.866	0.024	0.032	0.109	−0.048	−0.046	0.204	0.043	0.027	−0.026	0.001
A5−T8	H6a−O1	2.123	2.149	0.026	0.017	0.059	−0.020	−0.019	0.099	0.041	0.013	−0.010	0.002
A5−T8	N1−H3	1.689	1.708	0.019	0.057	0.094	−0.102	−0.097	0.293	0.054	0.037	−0.051	−0.014
A5−T8	H2−O2	2.700	2.741	0.041	0.006	0.021	−0.006	−0.005	0.032	0.093	0.004	−0.004	0.001
						Stacking (intrastrand)							
G4−A5	N1−N1	3.441	3.448	0.007	0.005	0.015	−0.003	−0.001	0.019	1.195	0.003	−0.003	0.000
G4−A5	N2−N3	3.295	3.300	0.005	0.006	0.018	−0.004	−0.003	0.025	0.267	0.004	−0.003	0.001
G4−A5	N3−C4	3.378	3.449	0.070	0.006	0.019	−0.002	−0.001	0.022	0.740	0.004	−0.003	0.001
G4−A5	N3−N9	3.386	3.430	0.043	0.006	0.017	−0.004	−0.000	0.021	15.572	0.004	−0.003	0.001
G4−A5	C4−C5	3.442	3.509	0.067	0.005	0.017	−0.002	−0.001	0.019	0.876	0.003	−0.003	0.001
G4−A5	N9−N7	3.416	3.485	0.069	0.005	0.016	−0.003	−0.001	0.020	3.588	0.004	−0.003	0.001
C9−T8	N4−N3	3.555	3.630	0.076	0.004	0.014	−0.003	−0.000	0.017	5.100	0.003	−0.002	0.001
C9−T8	C5−N1	3.567	3.610	0.042	0.005	0.013	−0.002	−0.001	0.016	1.064	0.003	−0.002	0.000
C9−T8	N1−O2	3.475	3.485	0.009	0.004	0.013	−0.002	−0.001	0.017	0.755	0.003	−0.002	0.000
						Stacking (interstrand)							
G4−T8	O6−O1	3.780	3.789	0.009	0.001	0.007	−0.001	−0.001	0.008	0.367	0.001	−0.001	0.000
A5−C9	H2−O2	2.753	2.835	0.082	0.006	0.021	−0.004	−0.004	0.029	0.233	0.004	−0.004	0.001

[a] The electron density was calculated at the B3LYP/6-311++G(d,p) level at the experimental geometry obtained from refs 48 and 49. All entries are in atomic units (au) except bond lengths (bl's) and bond path lengths (bpl's) and their differences which are in angstroms. [b] Labeling convention: see footnote of Table 1.

Besides the typical hydrogen bonds as X−H···O, very weak ones of the type X−H···C are also characterized in Table 10 but appear to be uncommon in DNA since only two were found in all the examined systems.

An interaction that occurs frequently mainly between the bases and the backbone and between backbone atoms and themselves is the H···H bonding interaction (to be distinguished[68−70] from dihydrogen bonding which was not found in this study). (The H···H bonding interaction is a nonelectrostatic stabilizing interaction between two hydrogen atoms carrying similar or identical charges of small magnitudes (close to electrical neutrality) and thus *is not* a variant of the hydrogen bond since it lacks a donor and an acceptor. In contrast, the dihydrogen bond represents the other end of the continuum in which one of the hydrogen atoms carries a positive charge and the other a negative charge[71] and *is* therefore a type of hydrogen bond where the hydrogen acceptor is a hydridic hydrogen atom.)[68,70] H···H bonding occurs, for example, in C−H···H−C even if one or both carbons are unsaturated or attached to electron withdrawing or donating groups.[68,69] In the DNA fragments considered here, 10 C−H···H−C bonding interactions were found, interactions which could contribute from 0.8 kcal/mol (ρ_b = 0.005 au) up to ~4 kcal/mol (ρ_b = 0.01 au) based on the extreme values of ρ_b (0.006 ± 0.003 au). The average over the 10 bonds given in Table 10 compares to the H···H bond arising in molecule **6**(*T*) of ref 68 (values in parentheses refer to the present work, all values are given in au except bond lengths): d(H···H) = 2.427 (2.386) Å, ρ_b = 0.005 (0.006), $\nabla^2\rho_b$ = 0.016 (0.021), ϵ = 0.062 (0.590), V_b = −0.002 (−0.003), and H_b = 0.001 (0.001).

Five weak O···O closed-shell interactions were found. This interaction was first described by Bone and Bader[72] and subsequently by a number of authors.[73−75] The O···O bond the properties in Table 10 agree very closely with those found in the silica polymorph coesite and obtained from periodic calculations by Gibbs et al.[73] (optimized crystal structures at the DFT(VWN,LDA) level using an 8-411G basis for oxygen and 65-111G(d) for silicon).[76] Gibbs et al. characterize several O···O bonding interactions for silica under several values of external pressure. Their values listed for the O···O bonding at the closest d(O···O) to the average separation given in Table 10 compare to the bond properties calculated in the present work

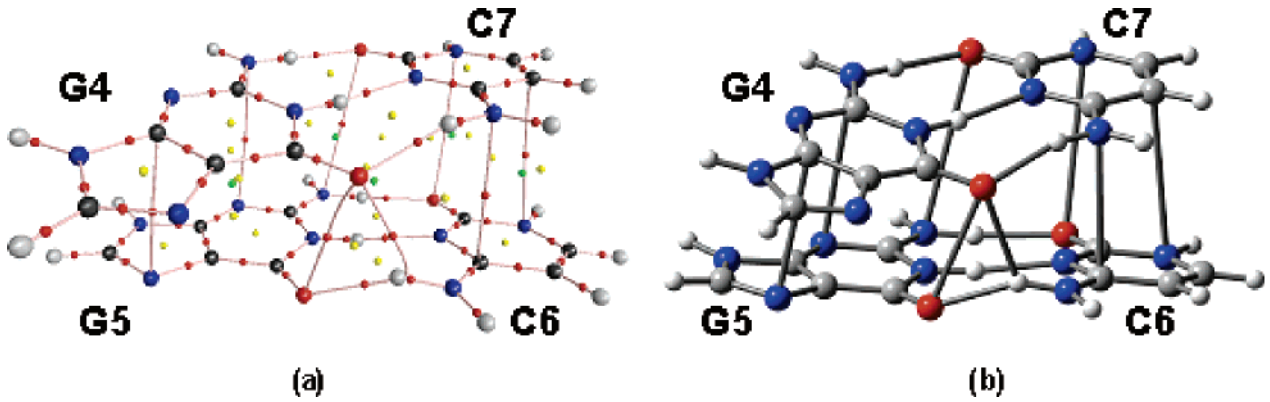

Figure 3. (a) Molecular graph of a GC/GC duplex of Watson−Crick dimers. The base numbering refers to the placement of the base in the experimental structure[47] from which the model has been taken. See the caption of Figure 1 for the color coding. The bond properties corresponding to this molecular graph are listed in Table 3. (b) A simplified ball-and-stick representation of the molecular graph where bond paths located in the electron density are represented by sticks.

TABLE 3: Closed-Shell Bonding in the $\downarrow\left|\begin{matrix}\text{G4−C7}\\ \text{G5−C6}\end{matrix}\right|\uparrow$ Dimer Duplex[a]

bases[b]	bond[b]	bl	bpl	bpl−bl	ρ_b	$\nabla^2\rho_b$	$\lambda1$	$\lambda2$	$\lambda3$	ϵ	G_b	V_b	H_b
Watson−Crick H-bonding													
G4−C7	H2a−O2	1.848	1.871	0.023	0.031	0.111	−0.047	−0.045	0.202	0.052	0.026	−0.025	0.001
G4−C7	H1−N3	1.831	1.852	0.021	0.040	0.103	−0.063	−0.059	0.225	0.069	0.029	−0.033	−0.003
G4−C7	O6−H4a	1.843	1.867	0.024	0.033	0.110	−0.049	−0.046	0.206	0.060	0.027	−0.026	0.001
G5−C6	H2a−O2	1.834	1.857	0.024	0.032	0.116	−0.049	−0.046	0.211	0.052	0.028	−0.026	0.001
G5−C6	H1−N3	1.832	1.853	0.021	0.039	0.103	−0.063	−0.059	0.225	0.070	0.029	−0.032	−0.003
G5−C6	O6−H4a	1.855	1.883	0.028	0.031	0.110	−0.046	−0.043	0.200	0.069	0.026	−0.025	0.001
Stacking (intrastrand)													
G4−G5	O6−O6	2.904	2.916	0.012	0.010	0.039	−0.008	−0.003	0.050	1.470	0.009	−0.008	0.001
G4−G5	N2−N3	3.742	3.747	0.006	0.003	0.009	−0.002	−0.001	0.012	0.139	0.002	−0.002	0.000
G4−G5	C4−N7	3.171	3.184	0.013	0.007	0.025	−0.004	−0.001	0.030	1.930	0.005	−0.004	0.001
C7−C6	N4−C4	3.107	3.146	0.039	0.008	0.027	−0.005	−0.002	0.034	1.461	0.006	−0.005	0.001
C7−C6	N1−O2	3.729	3.732	0.003	0.002	0.009	−0.001	−0.001	0.011	0.403	0.002	−0.001	0.000
C7−C6	C5−N1	3.618	3.648	0.030	0.004	0.011	−0.002	−0.002	0.015	0.195	0.002	−0.002	0.000
Stacking (interstrand)													
G4−C6	O6−H4a	2.262	2.419	0.156	0.014	0.055	−0.014	−0.010	0.079	0.433	0.012	−0.010	0.002
G5−C7	N2−O2	3.877	3.879	0.002	0.002	0.006	−0.001	−0.001	0.009	0.104	0.001	−0.001	0.000

[a] The electron density was calculated at the B3LYP/6-311++G(d,p) level at the experimental geometry obtained from ref 47. All entries are in atomic units (au) except bond lengths (bl's) and bond path lengths (bpl's) and their differences which are in angstroms. [b] Labeling convention: see footnote of Table 1.

(in parentheses) as follows: d(O···O) = 3.159 (3.154) Å, ρ_b = 0.007 (0.007) au, $\nabla^2\rho_b$ = 0.025 (0.029) au, $\lambda1$ = −0.005 (−0.006) au, $\lambda2$ = −0.004 (−0.004) au, and $\lambda3$ = 0.034 (0.038). The O···O bond properties in Table 10 also compare very well with several O···O bonding interactions found by Bone and Bader[72] in several conformations of a $(CO_2)_2$ dimer calculated at the MP2/TZ2P level of theory. In the parallel D_{2h} symmetry configuration of the $(CO_2)_2$, for example, the two CO_2 molecules are bonded by two closed-shell O···O interactions which are characterized by[72] (values in au): ρ_b = 0.006, $\nabla^2\rho_b$ = 0.030, $\lambda1$ = −0.005, $\lambda2$ = −0.002, $\lambda3$ = 0.038, ϵ = 1.121, and H_b = 0.002, values close to those in Table 10.

Another common interaction occurring between π-stacked bases is the closed-shell N···N bonding interaction. Seventeen such interactions were found in the four dimer duplexes and the four dinucleotides examined in the present work. The N···N bonding characterized here exhibits very similar characteristics to that found by Platts et al.[77] to link two π-stacked H−C≡C−C≡N molecules. These authors provide the following descriptors of the N···N bond compared to values from the present work (in parentheses), all values in au except distances: bpl = 3.458 (3.486) Å, ρ_b = 0.006 (0.005), and $\nabla^2\rho_b$ = 0.019 (0.015).

Nine weak C···C interactions were also identified. These are qualitatively similar but much weaker (significantly longer, lower ρ_b, softer curvatures, larger ellipticity) than a recently characterized similar interaction in a 1,8-difluoronaphthalene derivative (compound **3** in ref 78).

The C···C bond properties from ref 78 (compound **3**) are listed along with the averaged values from the present work (in parentheses), values are given in au except distances: d(C···C) = 2.853 (3.430) Å, ρ_b = 0.011 (0.005), $\nabla^2\rho_b$ = 0.039 (0.017) au, $\lambda1$ = −0.009 (−0.002), $\lambda2$ = −0.005 (−0.001), $\lambda3$ = 0.052 (0.019), ϵ = 0.646 (3.462), G_b = 0.008 (0.003), V_b = −0.007 (−0.003), and H_b = 0.002 (0.001).

Fourteen C···N bonding interactions were characterized. These are not dissimilar to a C···N bonding interaction reported by Platts et al. (along with the N···N interaction) between two π-stacked H−C≡C−C≡N molecules.[77] A comparison of Platt's reported properties and those from the present work (in parentheses) shows an excellent agreement (all values in au except distances): bpl = 3.703 (3.407) Å, ρ_b = 0.004 (0.006), and $\nabla^2\rho_b$ = 0.012 (0.019).

The N···O interaction is the longest bond found here, d(N···O) = 3.561 ± 0.164 Å, and is also the one exhibiting the least accumulation of density at the BCP, ρ_b = 0.003 ± 0.001 au. In

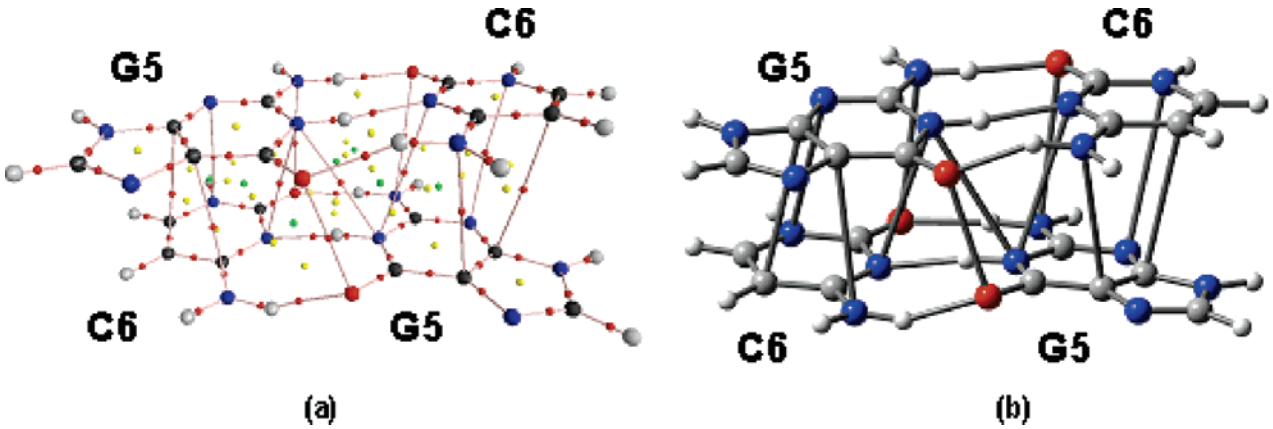

Figure 4. (a) Molecular graph of a GC/CG duplex of Watson−Crick dimers. The base numbering refers to the placement of the base in the experimental structure[47] from which the model has been taken. See the caption of Figure 1 for the color coding. The bond properties corresponding to this molecular graph are listed in Table 4. (b) A simplified ball-and-stick representation of the molecular graph where bond paths located in the electron density are represented by sticks.

TABLE 4: Closed-Shell Bonding in the $\downarrow\left|\begin{matrix}\text{G5−C6}\\ \text{C6−G5}\end{matrix}\right|\uparrow$ Dimer Duplex[a]

bases[b,c]	bond[b]	bl	bpl	bpl−bl	ρb	$\nabla^2\rho_b$	$\lambda1$	$\lambda2$	$\lambda3$	ϵ	G_b	V_b	H_b
Watson−Crick H-Bonding													
G5B−C6T	H2a−O2	1.834	1.858	0.024	0.032	0.114	−0.049	−0.046	0.209	0.051	0.027	−0.026	0.001
G5B−C6T	H1−N3	1.832	1.853	0.021	0.040	0.101	−0.063	−0.059	0.224	0.071	0.029	−0.032	−0.004
G5B−C6T	O6−H4a	1.855	1.881	0.026	0.031	0.111	−0.047	−0.044	0.201	0.065	0.027	−0.025	0.001
C5B−G6B	H2a−O2	1.834	1.876	0.042	0.032	0.110	−0.048	−0.045	0.203	0.061	0.027	−0.026	0.001
C5B−G6B	H1−N3	1.835	1.856	0.021	0.040	0.101	−0.063	−0.059	0.222	0.071	0.029	−0.032	−0.003
C5B−G6B	O6−H4a	1.851	1.858	0.007	0.032	0.114	−0.049	−0.047	0.209	0.052	0.027	−0.026	0.001
Stacking (intrastrand)													
G5T−C6B	N1−N3	3.451	3.461	0.010	0.005	0.016	−0.003	−0.002	0.020	0.861	0.003	−0.003	0.000
G5T−C6B	N2−O2	3.386	3.390	0.003	0.005	0.015	−0.003	−0.003	0.020	0.200	0.003	−0.003	0.000
G5T−C6B	N3−N1	3.512	3.522	0.010	0.004	0.014	−0.003	−0.001	0.017	1.306	0.003	−0.003	0.000
G5T−C6B	C4−C5	3.417	3.432	0.015	0.006	0.017	−0.003	−0.000	0.021	8.866	0.004	−0.003	0.001
G5T−C6B	C5−N4	3.275	3.297	0.022	0.007	0.021	−0.004	−0.003	0.028	0.485	0.005	−0.004	0.001
C6T−G5B	N4−C5	3.257	3.279	0.022	0.007	0.022	−0.004	−0.003	0.029	0.418	0.005	−0.004	0.001
C6T−G5B	C5−C4	3.381	3.396	0.014	0.006	0.018	−0.003	−0.001	0.022	4.234	0.004	−0.003	0.001
C6T−G5B	N1−N3	3.503	3.508	0.004	0.005	0.013	−0.003	−0.002	0.018	0.722	0.003	−0.003	0.000
C6T−G5B	O2−N2	3.435	3.439	0.004	0.004	0.014	−0.003	−0.002	0.019	0.264	0.003	−0.003	0.000
C6T−G5B	N3−N1	3.453	3.463	0.010	0.005	0.015	−0.003	−0.002	0.020	0.831	0.003	−0.003	0.000
Stacking (interstrand)													
G5T−G5B	N1−N1	3.381	3.393	0.012	0.005	0.017	−0.004	−0.002	0.022	0.984	0.004	−0.003	0.001
G5T−G5B	O6−O6	2.758	2.761	0.003	0.012	0.047	−0.010	−0.010	0.066	0.025	0.010	−0.009	0.001

[a] The electron density was calculated at the B3LYP/6-311++G(d,p) level at the experimental geometry obtained from ref 47. All entries are in atomic units (au) except bond lengths (bl's) and bond path lengths (bpl's) and their differences which are in angstroms. [b] Labeling convention: see footnote of Table 1. [c] "T" refers to bases at the top of Figure 4, and "B" refers to bases at the bottom of the figure.

view of these characteristics, this bonding probably has insignificant energetic consequences.

In the following section, we will discuss the peculiarities of the bonding in each separate DNA fragment under consideration.

5.1.2.1. Ade5 Thy8/Ade6 Thy7 Dimer Duplex. The molecular graph of this system is given in Figure 1 and bond properties of the weak interactions linking the two base pairs can be found in Table 1. As can be seen from the values of ρ_b, all of the intrastrand and interstrand interactions in this duplex, 11 in total, are very weak. The duplex is held by nine intrastrand and two interstrand interactions.

A hydrogen bond path links Thy8 to Ade6, namely, Thy8-(O2)···(H2)Ade6, a particularly interesting interstrand interaction since it is slightly stronger than the newly characterized third WC hydrogen bonding within the AT dimer itself. This interstrand interaction is characterized by a bl = 2.741 Å and ρ_b = 0.006 au, to be compared with the WC Ade5(H2)···(O2)-Thy8 with the corresponding values of 2.874 Å and 0.005 au, respectively. This interstrand bonding can, thus, be expected to contribute ∼1 kcal to the binding of the duplex.

Interestingly, atom N6 of Ade5 is involved in an intrastrand bonding interaction with N6 of the following Ade6 in the same strand and simultaneously shares a bond path with the oxygen O1 belonging to the Thy7 base on the opposite strand and belonging to the adjacent dimer. The Ade5(N6)···(O1)Thy7 bond path is not topologically stable as can be seen from the relatively large ellipticity, the similarity of ρ_b = 0.003 au to the value of the electron density at the neighboring RCP, ρ_{rcp} = 0.002 au, and the short distance separating this BCP from the associated RCP (0.594 Å). This BCP and the neighboring RCP may coalesce and annihilate one another upon relatively minor geometrical changes such as those accompanying molecular vibrations.

5.1.2.2. Gua4 Cyt9/Ade5 Thy8 Dimer Duplex. The molecular graph of this dimer duplex is depicted in Figure 2, and the bonding is characterized in Table 2. Eleven weak intra- and interstrand interactions arise in this dimer duplex. There exist several types of weak interstrand interactions: five N···N, two C···N, one C···C, and one N···O. The interstrand hydrogen bond Ade5(H2)···(O2)Cyt9 is comparable yet slightly weaker than

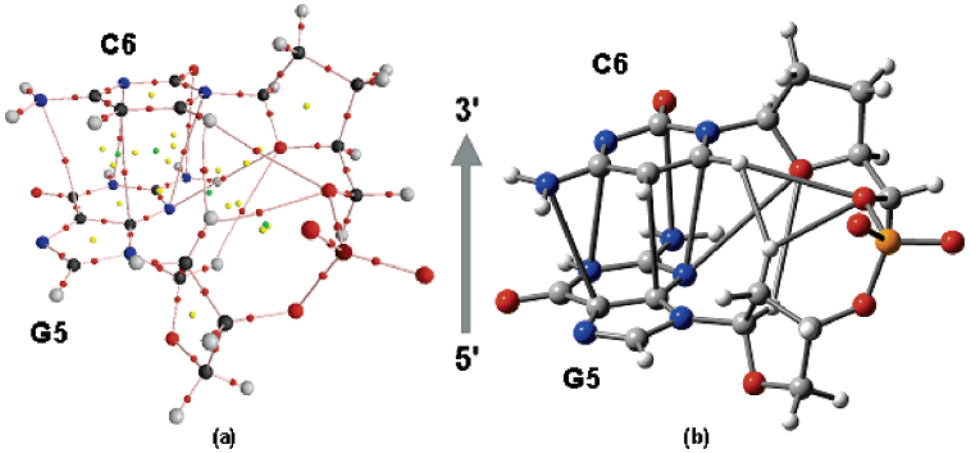

Figure 5. (a) Molecular graph of a G/C duplex of single nucleobases attached to their backbone. The base numbering refers to the placement of the base in the experimental structure[47] from which the model has been taken. See the caption of Figure 1 for the color coding. The bond properties corresponding to this molecular graph are listed in Table 5. (b) A simplified ball-and-stick representation of the molecular graph where bond paths located in the electron density are represented by sticks.

TABLE 5: Closed-shell Bonding in the Dinucleotide $\left|\begin{matrix}\text{C6}\\ \text{G5}\end{matrix}\right|\uparrow$ with the Backbone[a]

moiety[b]	bond[b]	bl	bpl	bpl−bl	ρ_b	$\nabla^2\rho_b$	$\lambda1$	$\lambda2$	$\lambda3$	ϵ	G_b	V_b	H_b
						Stacking							
G5−C6	C5−N4	3.257	3.271	0.014	0.007	0.022	−0.004	−0.003	0.029	0.287	0.005	−0.004	0.001
G5−C6	C4−C5	3.381	3.397	0.016	0.006	0.018	−0.003	−0.001	0.022	4.234	0.004	−0.003	0.001
G5−C6	N3−N1	3.503	3.519	0.016	0.004	0.014	−0.003	−0.001	0.017	1.404	0.003	−0.002	0.000
G5−C6	O2−N2	3.435	3.438	0.003	0.004	0.013	−0.003	−0.002	0.019	0.257	0.003	−0.003	0.000
G5−C6	N1−N3	3.453	3.462	0.009	0.005	0.015	−0.003	−0.002	0.019	0.773	0.003	−0.003	0.000
						C6−Backbone							
C6−BB(C6)	H6−O5′	2.965	2.999	0.034	0.004	0.013	−0.002	−0.001	0.016	1.137	0.003	−0.002	0.001
C6−BB(G5)	H6−H2′b	2.184	2.275	0.092	0.007	0.022	−0.007	−0.005	0.034	0.233	0.004	−0.003	0.001
						G5−Backbone							
G5−BB(C6)	N3−O4′	3.674	3.680	0.006	0.002	0.010	−0.002	−0.001	0.012	0.840	0.002	−0.001	0.001
						Backbone−Backbone							
BB(G5)−BB(C6)	H2′b−O5′	2.488	2.524	0.036	0.010	0.035	−0.009	−0.006	0.050	0.494	0.008	−0.006	0.001
BB(C6)−BB(G5)	O4′−H1′	3.300	3.334	0.034	0.002	0.007	−0.001	−0.001	0.009	0.161	0.001	−0.001	0.000

[a] The electron density was calculated at the B3LYP/6-311++G(d,p) level at the experimental geometry obtained from ref 47. All entries are in atomic units (au) except bond lengths (bl's) and bond path lengths (bpl's) and their differences which are in angstroms. [b] Labeling convention: The column labeled "bond" lists the two atoms involved in the bonding, the first atom belonging to the first nucleotide listed under "moiety" and the second belonging to the second nucleotide. When the base label is listed, the atom belongs to the base, but when BB(X) is listed, the atom belongs to the backbone of the nucleotide in which the base X exists. For example, the first entry under "backbone−backbone" (BB(G5)−BB(C6), H2′b−O5′) means that the bonding is between atom H2′b belonging to the backbone of the *nucleotide* G5 and atom O5′ belonging to backbone of the *nucleotide* C6. The labeling of the stacking interaction follows the same conventions described in the footnote of Table 1. Atom numbering schemes of the bases and the backbone are given in Figures 10 and 11, respectively, of the Appendix. The same conventions are adopted in Tables 6−8.

the WC AT-III as can be seen from a direct comparison of the respective entries in Table 2. The Gua4(O6)···(O1)Thy8 bond is extremely weak and topologically unstable and could be an artifact of the level of theory.

5.1.2.3. Gua4 Cyt7/Gua5 Cyt6 Dimer Duplex. Figure 3 displays the molecular graph of this dimer duplex, and Table 3 lists the corresponding bond properties of the weak bonding interactions. This duplex is held by eight weak interactions four of which are slightly stronger than the similar ones encountered in the other dimer duplexes. The relatively stronger interactions include: (1) two intrastrand C···N interactions, (2) an intrastrand dioxygen interaction Gua4(O6)···(O6)Gua5, which exhibits a relatively significant accumulation of density at the BCP (ρ_b = 0.01 au), higher than its much longer counterpart in the previous dimer duplex, and (3) an interstrand hydrogen bond, namely, Gua4(O6)···(H4a)Cyt6, with ρ_b = 0.014 au. The dioxygen interaction and this hydrogen bond are the strongest interactions on the basis of the accumulation of density at their BCPs. Both of these two stacking interactions fall on the same side of the dimer duplex causing a significant roll of the Gua4Cyt7 dimer with respect to the Gua5Cyt6 dimer, a roll characterized by a smaller separation between the two stacked dimers from the major-groove side than the separation from the minor-groove side. The intrastrand dioxygen Gua4(O6)···(O6)Gua5 interaction, the interstrand hydrogen bonding Gua4(O6)···(H4a)Cyt6, and the WC hydrogen bond G5(O6)···(H4a)C6 close a three-membered ring composed of the atoms Gua4(O6), Gua5(O6), and Cyt6(H4a) and characterized by a central RCP not far from the centroid of the triangle, ρ_{rcp} = 0.010 au.

5.1.2.4. Gua5 Cyt6/Cyt6′ Gua5′ Dimer Duplex. Figure 4 displays the molecular graph of the dimer duplex, the weak bonding of which is characterized in Table 4. There exist 10 intra- and 2 interstrand weak bonding interactions. The bonding interactions are quite varied, including N···N, N···O, C···C, C···N, and O···O interactions. Two C···N bonding interactions exhibit the highest accumulation of density at the BCP among the interstrand interactions (ρ_b = 0.007 au). An interstrand dioxygen interaction is shorter and has a higher ρ_b than the one occurring in the Gua4Cyt7/Gua5Cyt6 dimer duplex (compare the entries for the dioxygen interactions in Table 3 with those in Table 4). It is interesting to note that the nitrogen atoms N1 of each of the two guanine bases are involved, each, in two

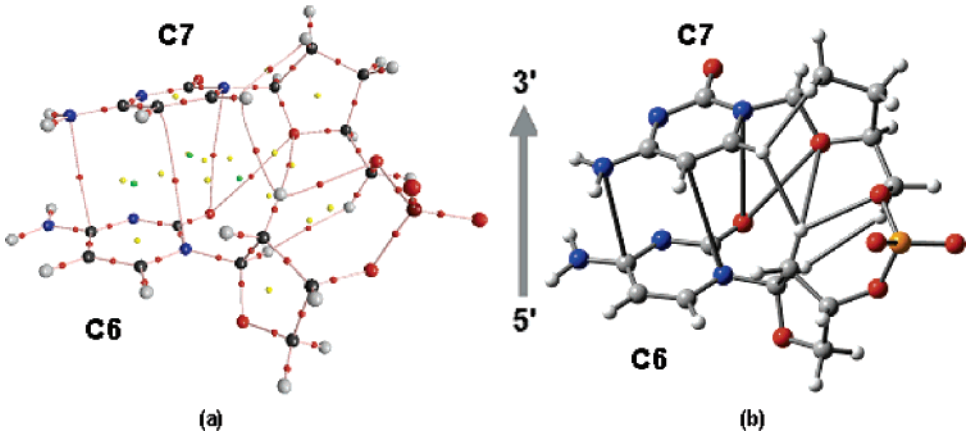

Figure 6. (a) Molecular graph of a C/C duplex of single nucleobases attached to their backbone. The base numbering refers to the placement of the base in the experimental structure[47] from which the model has been taken. See the caption of Figure 1 for the color coding. The bond properties corresponding to this molecular graph are listed in Table 6. (b) A simplified ball-and-stick representation of the molecular graph where bond paths located in the electron density are represented by sticks.

TABLE 6: Closed-Shell Bonding in the Dinucleotide $\left|\begin{matrix}\mathbf{C7}\\\mathbf{C6}\end{matrix}\right|\uparrow$ with the Backbone[a]

moiety[b]	bond[b]	bl	bpl	bpl−bl	ρ_b	$\nabla^2\rho_b$	$\lambda1$	$\lambda2$	$\lambda3$	ϵ	G_b	V_b	H_b
						Stacking							
C7−C6	N4−C4	3.107	3.113	0.006	0.008	0.028	−0.005	−0.002	0.035	1.269	0.006	−0.005	0.001
C7−C6	N1−O2	3.729	3.736	0.008	0.002	0.009	−0.001	−0.001	0.010	0.425	0.002	−0.001	0.000
C7−C6	C5−N1	3.618	3.637	0.018	0.004	0.011	−0.002	−0.001	0.015	0.357	0.002	−0.002	0.000
						C7−Backbone							
C7−BB(C7)	H6−H2′a	2.086	2.443	0.357	0.012	0.049	−0.010	−0.004	0.063	1.873	0.010	−0.008	0.002
C7−BB(C6)	H6−H2′b	2.356	2.497	0.141	0.005	0.017	−0.004	−0.004	0.025	0.257	0.004	−0.003	0.001
						C6−Backbone							
C6−BB(C7)	O2−O4′	3.423	3.429	0.006	0.003	0.013	−0.002	−0.002	0.018	0.037	0.003	−0.002	0.001
						Backbone−Backbone							
BB(C7)−BB(C6)	O4′−H2′b	3.036	3.059	0.024	0.003	0.013	−0.002	−0.000	0.015	3.764	0.003	−0.002	0.001
BB(C7)−BB(C6)	O5′−H2′b	2.350	2.379	0.029	0.014	0.045	−0.014	−0.012	0.071	0.197	0.010	−0.009	0.001
BB(C7)−BB(C6)	H5′−H1′	2.474	2.523	0.049	0.004	0.012	−0.003	−0.003	0.018	0.131	0.002	−0.002	0.000

[a] The electron density was calculated at the B3LYP/6-311++G(d,p) level at the experimental geometry obtained from ref 47. All entries are in atomic units (au) except bond lengths (bl's) and bond path lengths (bpl's) and their differences which are in angstroms. [b] Labeling convention: see footnote of Table 5.

weak N···N bonding with N3 of the cytosine of its adjacent dimer on the same strand. Also, the N1 atoms of the two guanine bases are linked by a bond path. The result is a zigzag of N···N bonds: Cyt6(N3)···Gua5(N1)···Gua5′(N1)···Cyt6′(N3). These bonding interactions along with the two WC-II bonds result in the closure of two four-membered rings of triangular geometry (since the three members belonging to the WC-II hydrogen bond fall roughly on the same line). The two resulting RCPs have $\rho_{rcp} = 0.004$ au, not much smaller than the ρ_b of the N···N bonds ($\rho_b \sim 0.005$ au).

On the basis of ρ_b, the O···O interstrand interaction is the strongest interaction in this dimer duplex. This bond path is topologically stable, the closest RCP being 1.31 Å away. Also, there is a significant difference between the ρ_b of this interaction ($\rho_b = 0.012$ au) and the density in the three closest RCPs, $\rho_{rcp} \sim 0.003$ au in all three RCPs.

5.2. Dinucleotides. The dinucleotides (monomer duplexes) considered in this study are

$\left|\begin{matrix}\mathbf{C6}\\\mathbf{G5}\end{matrix}\right|\uparrow$ (Table and Figure 5), $\left|\begin{matrix}\mathbf{C7}\\\mathbf{C6}\end{matrix}\right|\uparrow$ (Table and Figure 6),

$\left|\begin{matrix}\mathbf{C5}\\\mathbf{C4}\end{matrix}\right|\uparrow$ (Table and Figure 7), and $\left|\begin{matrix}\mathbf{T7}\\\mathbf{A6}\end{matrix}\right|\uparrow$ (Table and Figure 8)

In the above notation, the numbers indicate the position of the base in the DNA sequence in the original experimental α-helix from which it was extracted and the arrows point in the 5′ → 3′ direction. For simplicity, we will adopt the following more compact notation for the above dimer duplexes: Gua5/Cyt6, Cyt6/Cyt7, Cyt4/Cyt5, and Ade6/Thy7, respectively. In the following, we shall concentrate on the base−backbone and backbone−backbone interactions, since we have already examined the π-stacking interactions in detail. The π-stacking interactions in each case are almost identical to their counterparts determined for the dimer duplexes, with the very small numerical differences between the properties of interaction determined for the same stacked bases being due to the change in the electronic environment (backbone instead of the WC complementary base).

5.2.1. Gua5/Cyt6 Dinucleotide. The stacking interactions in Table 5 are almost identical to their counterparts listed in Table 4 (6th−10th entry under "Stacking (intrastrand)"). In addition to π-stacking, the dinucleotide exhibits several base−backbone bonding interactions. A weak hydrogen bonding interaction links H6 of cytosine to the backbone O5′ of its own nucleotide. This hydrogen bond is very weak and being too close in space to two ring critical points, is topologically unstable. More significantly, the same hydrogen atom participates in a hydrogen−hydrogen bonding interaction linking cytosine to the sugar atom H2′b belonging to the guanosine nucleotide. This H−H bonding

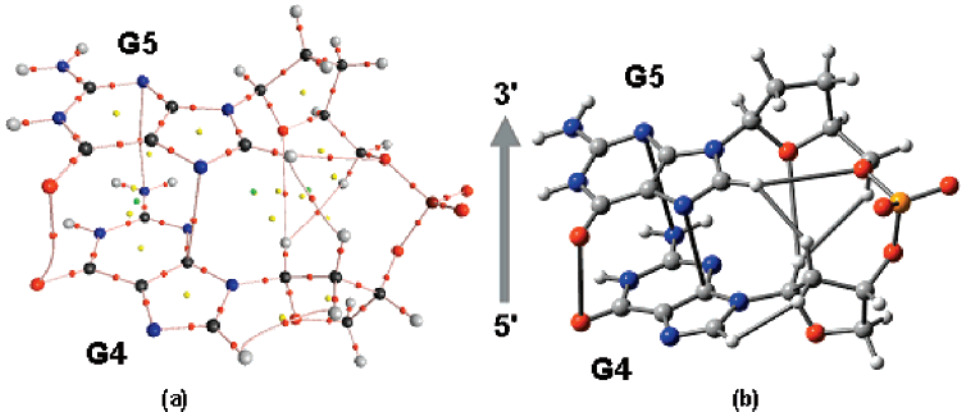

Figure 7. (a) Molecular graph of a G/G duplex of single nucleobases attached to their backbone. The base numbering refers to the placement of the base in the experimental structure[47] from which the model has been taken. See the caption of Figure 1 for the color coding. The bond properties corresponding to this molecular graph are listed in Table 7. (b) A simplified ball-and-stick representation of the molecular graph where bond paths located in the electron density are represented by sticks.

TABLE 7: Closed-Shell Bonding in the Dinucleotide $\left|\begin{matrix}\text{G5}\\\text{G4}\end{matrix}\right|\uparrow$ with the Backbone[a]

moiety[b]	bond[b]	bl	bpl	bpl−bl	ρ_b	$\nabla^2\rho_b$	$\lambda1$	$\lambda2$	$\lambda3$	ϵ	G_b	V_b	H_b
						Stacking							
G5−G4	O6−O6	2.904	2.972	0.068	0.010	0.037	−0.007	−0.003	0.047	1.761	0.008	−0.007	0.001
G5−G4	N3−N2	3.742	3.754	0.012	0.003	0.009	−0.002	−0.001	0.012	0.146	0.002	−0.002	0.000
G5−G4	N7−C4	3.171	3.183	0.012	0.007	0.025	−0.004	−0.002	0.030	1.716	0.005	−0.004	0.001
						G4−Backbone							
G4−BB(G4)	H8−H2′a	2.162	2.478	0.315	0.010	0.039	−0.009	−0.003	0.051	2.297	0.008	−0.006	0.002
						G5−Backbone							
G5−BB(G5)	H8−O5′	3.047	3.074	0.026	0.003	0.011	−0.002	−0.002	0.015	0.371	0.002	−0.002	0.001
G5−BB(G4)	H8−H2′b	2.196	2.263	0.068	0.006	0.020	−0.006	−0.005	0.031	0.138	0.004	−0.003	0.001
						Backbone−Backbone							
BB(G5)−BB(G4)	O4′−H1′	3.192	3.213	0.021	0.002	0.008	−0.001	−0.001	0.011	0.102	0.002	−0.001	0.000
BB(G5)−BB(G4)	H5′−H1′	2.754	2.806	0.052	0.002	0.008	−0.002	−0.001	0.010	0.469	0.002	−0.001	0.000

[a] The electron density was calculated at the B3LYP/6-311++G(d,p) level at the experimental geometry obtained from ref 47. All entries are in atomic units (au) except bond lengths (bl's) and bond path lengths (bpl's) and their differences which are in angstroms. [b] Labeling convention: see footnote of Table 5.

is still very weak but more significant in terms of electron density at the BCP ($\rho_b = 0.007$ au). A weak interaction links N3 of guanine to O4 of the cytidine, but this bonding is probably unstable and may disappear upon changing the basis set or theoretical method.

Finally, this DNA fragment exhibits backbone-to-backbone (BB) hydrogen bonding. The most significant BB interaction is that between H2′b of the sugar of the guanosine and the O5′ of the phosphate belonging to the cytidine ($\rho_b = 0.01$ au), which is still considered a weak hydrogen bond. This results in a closed three-membered ring structure involving Cyt6(O5′), Gua5(H2′b), and Cyt6(H6). The H6 atom of the cytosine is thus involved in a bifurcated weak bond to the O5′ of its own backbone and to the H2′b of the sugar of the neighboring nucleotide. The same can be said about atom H2′b belonging to the deoxyribose sugar of the guanosine nucleotide. Both hydrogen atoms are involved simultaneously in a hydrogen−hydrogen bond (to each other), and both are also simultaneously involved in weak hydrogen bonding to the phosphate oxygen of the cytidine closing a triangular three-membered ring.

5.2.2. Cyt6/Cyt7 Dinucleotide. A comparison of the stacking interactions in Table 6 with those listed in Table 3 reveals that they are almost identical as expected. In addition to these interactions, a similar pattern of bifurcated bonding at H6 of cytosine and at H2′b of the sugar moiety of the cytidine found in the previous dinucleotide is also found here. Atom H2′b of Cyt6 is involved in a weak hydrogen bond ($\rho_b = 0.014$ au) linking it to O5′ of Cyt7, and at the same time, it is also bonded to H6 of Cyt7 ($\rho_b = 0.005$ au) and finally to O4′ of the sugar of Cyt7 ($\rho_b = 0.003$ au). Atom H2′b is thus involved in a trifurcated weak bonding arrangement. Atom H6 of Cyt7 is involved in a bifurcated weak bond, on one hand, to H2′b of the Cyt6 sugar and, on the other hand, to H2′a of the sugar belonging to its own nucleotide Cyt7. The Cyt7(H6)−Cyt7-(H2′a) hydrogen−hydrogen bonding and the Cyt7(O5′)−Cyt6-(H2′b) hydrogen bonding interactions are the only two closed-shell interactions of some significance found in this dinucleotide. The rest are weaker as can be gleaned from the values of ρ_b listed in Table 6.

5.2.3. Gua4/Gua5 Dinucleotide. Again, a comparison of the stacking interactions listed in Table 7 with the corresponding ones in Table 3 reveals little or no influence induced by the change in the electronic environment. The only two weak interactions of some significance found here are (1) a hydrogen−hydrogen bond linking H8 of Gua4 to its own nucleotide's H2′a, a bond which exhibits a $\rho_b = 0.010$ au, which can thus be considered weak and also unstable due to its close proximity to a ring critical point (as can be seen from Figure 7a) and (2) a second hydrogen−hydrogen bond linking H8 of Gua5 to H2′b of the other nucleotide, $\rho_b = 0.006$ au.

5.2.4. Ade6/Thy7 Dinucleotide. The closed-shell bonding in this dinucleotide is illustrated in Figure 8 and listed in Table 8. There is no corresponding dimer duplex studied here to compare with the stacking interactions in this dinucleotide, but

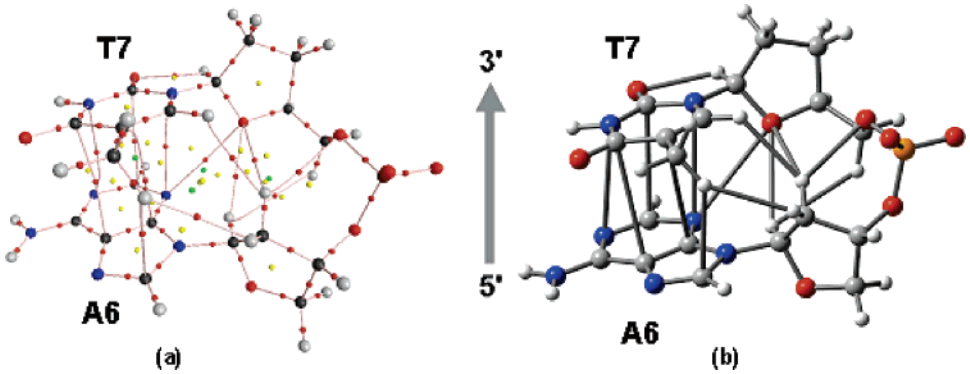

Figure 8. (a) Molecular graph of an A/T duplex of single nucleobases attached to their backbone. The base numbering refers to the placement of the base in the experimental structure[48,49] from which the model has been taken. See the caption of Figure 1 for the color coding. The bond properties corresponding to this molecular graph are listed in Table 8. (b) A simplified ball-and-stick representation of the molecular graph where bond paths located in the electron density are represented by sticks.

TABLE 8: Closed-Shell Bonding in the Dinucleotide $\left|\begin{matrix}\text{T7}\\ \text{A6}\end{matrix}\right|\uparrow$ with the Backbone[a]

moiety[b]	bond[b]	bl	bpl	bpl−bl	ρ_b	$\nabla^2\rho_b$	$\lambda1$	$\lambda2$	$\lambda3$	ϵ	G_b	V_b	H_b
						Stacking							
T7−A6	N3−N1	3.429	3.466	0.037	0.005	0.015	−0.003	−0.001	0.019	1.773	0.003	−0.003	0.000
T7−A6	C4−C5	3.471	3.494	0.023	0.004	0.014	−0.002	−0.001	0.017	2.773	0.003	−0.002	0.001
T7−A6	C5−C4	3.576	3.695	0.119	0.005	0.013	−0.002	−0.001	0.016	2.229	0.003	−0.002	0.001
T7−A6	N1−N3	3.398	3.417	0.019	0.005	0.015	−0.003	−0.002	0.020	1.041	0.003	−0.003	0.000
T7−A6	C2−C2	3.312	3.377	0.065	0.005	0.019	−0.001	−0.001	0.021	0.730	0.004	−0.003	0.001
T7−A6	H5b−C8	2.866	2.895	0.029	0.005	0.016	−0.003	−0.003	0.022	0.108	0.003	−0.003	0.001
						T7−Backbone							
T7−BB(T7)	O2−H1′	2.194	2.287	0.093	0.021	0.087	−0.022	−0.008	0.117	1.848	0.019	−0.015	0.003
T7−BB(A6)	H6−H2′b	2.379	2.463	0.084	0.005	0.016	−0.004	−0.004	0.024	0.050	0.003	−0.003	0.001
T7−BB(A6)	H5b−H2′a	2.492	2.585	0.093	0.004	0.013	−0.003	−0.003	0.019	0.069	0.003	−0.002	0.001
						A6−Backbone							
A6−BB(T5)	N3−O4′	3.347	3.357	0.009	0.005	0.017	−0.003	−0.003	0.023	0.091	0.003	−0.003	0.001
						Backbone−Backbone							
BB(T7)−BB(A6)	O4′−H1′	2.845	2.888	0.043	0.005	0.017	−0.004	−0.003	0.023	0.306	0.003	−0.003	0.001
BB(T7)−BB(A6)	O4′−H2′b	2.976	2.993	0.018	0.004	0.013	−0.002	−0.002	0.017	0.385	0.003	−0.002	0.001
BB(T7)−BB(A6)	H5′−H1′	2.780	3.051	0.271	0.003	0.010	−0.002	−0.001	0.013	0.382	0.002	−0.001	0.001
BB(T7)−BB(A6)	O5′−H2′b	2.491	2.526	0.035	0.011	0.034	−0.010	−0.006	0.050	0.577	0.008	−0.007	0.001

[a] The electron density was calculated at the B3LYP/6-311++G(d,p) level at the experimental geometry obtained from refs 48 and 49. All entries are in atomic units (au) except bond lengths (bl's) and bond path lengths (bpl's) and their differences which are in angstroms. [b] Labeling convention: see footnote of Table 5.

TABLE 9: Average Properties for the Watson−Crick Hydrogen Bonding Interactions[a]

	short label	bl	bpl	bpl−bl	ρ_b	ρ_b[b 66]	$\nabla^2\rho_b$	$\lambda1$	$\lambda2$	$\lambda3$	ϵ	G_b	V_b	H_b	$-(1/2)V_b$[c 66]	E[d 55]
AT															−12.7[e]	−14.7[f]
H6a−O1	I	2.116	2.141	0.025	0.017	0.026	0.061	−0.022	−0.021	0.103	0.046	0.013	−0.011	0.002	−6.1	−5.9
N1−H3	II	1.725	1.744	0.019	0.052	0.041	0.093	−0.091	−0.086	0.271	0.055	0.034	−0.045	−0.011	(−5.8)[g]	−4.8
H2−O2	III	2.743	2.790	0.047	0.006	0.004	0.020	−0.005	−0.005	0.030	0.108	0.004	−0.003	0.001	−0.8	−1.0
CG															−25.7[h]	−29.3[i]
O6−H4a	I	1.849	1.871	0.022	0.032	0.037	0.111	−0.048	−0.045	0.204	0.058	0.027	−0.026	0.001	−10.5	−5.4
H1−N3	II	1.854	1.876	0.021	0.038	0.033	0.100	−0.059	−0.055	0.215	0.072	0.028	−0.030	−0.003	(−8.9)[g]	−8.8
H2a−O2	III	1.867	1.895	0.028	0.030	0.027	0.107	−0.045	−0.042	0.194	0.061	0.025	−0.024	0.001	−6.3	−12.5

[a] Averaged over three different AT base pairs and five GC base pairs. All entries are in atomic units (au) except bond lengths (bl's) and bond path lengths (bpl's) and their differences which are in angstroms, and energies entered in the last two columns are in kcal/mol. [b] Values of ρ_b taken from ref 66, calculated at the B3LYP/6-311++G(d,p)//6-31+G(d,p). [c] Values of $-(1/2)V_b$ in kcal/mol taken from ref 66 and which can be used to estimate X−H···O hydrogen bond energies according to the findings in ref 58. [d] Estimates of E are taken from ref 55 and calculated at the B3LYP/D95(d,p) without BSSE correction (the closest level of theory to the one used in the present paper); see text. [e] Total binding energy of the AT dimer calculated at the B3LYP/6-311++G(d,p)//6-31+G(d,p) level and taken from ref 66. [f] Total binding energy of the AT dimer calculated at the B3LYP/D95G(d,p) level and taken from ref 55. [g] Values between brackets were calculated by difference. [h] Total binding energy of the GC dimer calculated at the B3LYP/6-311++G(d,p)//6-31+G(d,p) level and taken from ref 66. [i] Total binding energy of the GC dimer calculated at the B3LYP/D95G(d,p) level and taken from ref 55.

these are not expected to differ significantly. The π-stacking interactions between the adenine and the thymine are similar to the other closed-shell interactions encountered in the other duplexes. Two N−N, three C−C, and one C−H closed-shell π-stacking interactions exist between adenine and thymine with 0.004 au $< \rho_b <$ 0.005 au.

One of thymine's oxygen atoms, O2, acts as an acceptor in a weak hydrogen bond (ρ_b = 0.021 au) from the sugar of its

TABLE 10: Average Properties for the Different Classes of Weak Interactions in this Study other than the Watson−Crick Hydrogen Bonding

bond	n^a		bl	bpl	bpl−bl	ρ_b	$\nabla^2\rho_b$	$\lambda1$	$\lambda2$	$\lambda3$	ϵ	G_b	V_b	H_b
X−H···C	2	avg	2.872	2.908	0.036	0.005	0.016	−0.003	−0.003	0.022	0.199	0.003	−0.003	0.001
		std	0.006	0.013	0.007	0.000	0.000	0.000	0.000	0.000	0.091	0.000	0.000	0.000
X−H···O	26	avg	2.386	2.427	0.041	0.017	0.060	−0.022	−0.020	0.102	0.425	0.014	−0.013	0.001
		std	0.502	0.506	0.033	0.012	0.043	0.020	0.019	0.082	0.775	0.010	0.010	0.001
H···H	10	avg	2.386	2.538	0.152	0.006	0.021	−0.005	−0.003	0.029	0.590	0.004	−0.003	0.001
		std	0.230	0.224	0.111	0.003	0.013	0.003	0.001	0.016	0.764	0.003	0.002	0.001
C···C	9	avg	3.430	3.505	0.075	0.005	0.017	−0.002	−0.001	0.019	3.462	0.003	−0.003	0.001
		std	0.087	0.169	0.098	0.001	0.002	0.001	0.000	0.002	2.317	0.000	0.000	0.000
C···N	14	avg	3.357	3.407	0.050	0.006	0.019	−0.003	−0.002	0.024	0.908	0.004	−0.003	0.001
		std	0.184	0.221	0.074	0.002	0.006	0.001	0.001	0.007	0.544	0.001	0.001	0.000
N···N	17	avg	3.466	3.486	0.020	0.005	0.015	−0.003	−0.001	0.019	2.103	0.003	−0.003	0.000
		std	0.116	0.118	0.022	0.001	0.002	0.001	0.001	0.003	3.583	0.001	0.000	0.000
N···O	11	avg	3.561	3.569	0.007	0.003	0.012	−0.002	−0.002	0.015	0.387	0.002	−0.002	0.000
		std	0.164	0.164	0.008	0.001	0.003	0.001	0.001	0.004	0.240	0.001	0.001	0.000
O···O	5	avg	3.154	3.173	0.020	0.007	0.029	−0.006	−0.004	0.038	0.732	0.006	−0.005	0.001
		Std	0.386	0.380	0.024	0.004	0.016	0.003	0.003	0.022	0.738	0.004	0.003	0.000

[a] n is the number of bonding interactions included in the averaging.

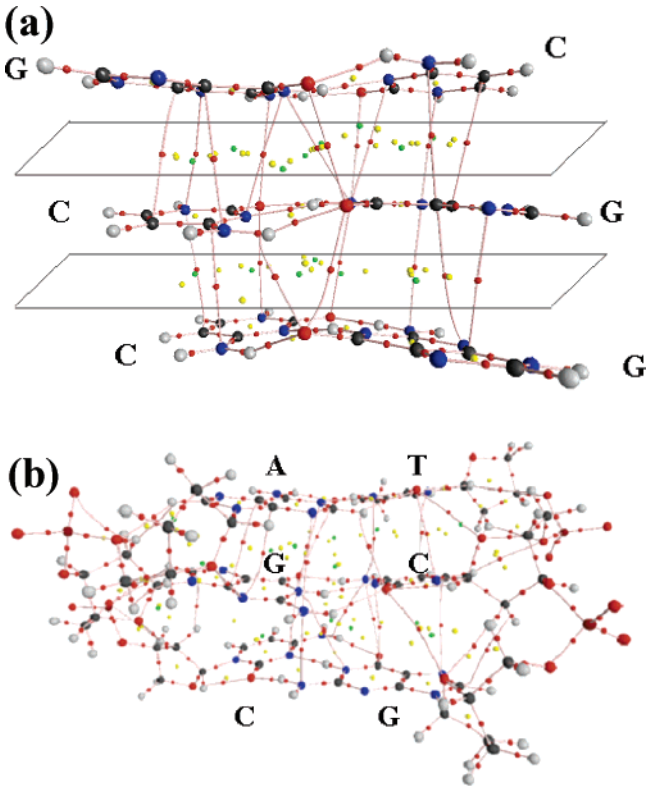

Figure 9. (a) View of the molecular graph of a triplex of Watson and Crick base pairs GC/CG/CG (from top to bottom). The bases were obtained from the middle section of the experimental structure reported in ref 47, and all six dangling bonds have been saturated with hydrogen atoms. See the caption of Figure 1 for the color coding. The extended network of bonding interaction linking neighboring bases beyond one base pair continues ad infinitum. The plane of the figure has been tilted so that the bases pairs are roughly perpendicular to the plane of the drawing. The reader is asked to note that all the critical points between any neighboring base stacks (BCP, RCP, and CCP) all fall approximately on a plane between the π-stacked base pairs. (b) Another section of the DNA molecule (AT/GC/CG) with the backbone atoms showing the complex web of weak closed-shell bonding interaction between the base pairs, between the bases and the backbone, and among backbone atoms and themselves.

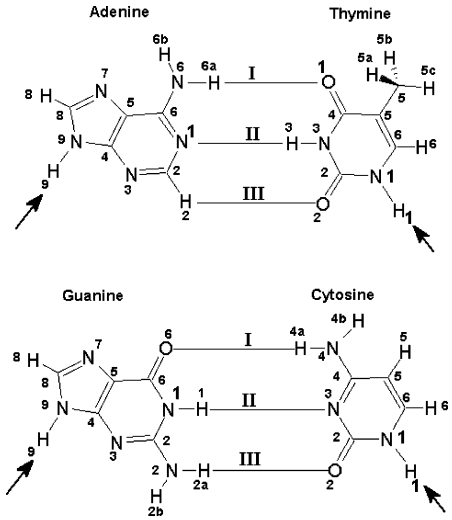

Figure 10. Numbering scheme of the nucleic acid bases in Watson-and-Crick base pairs.

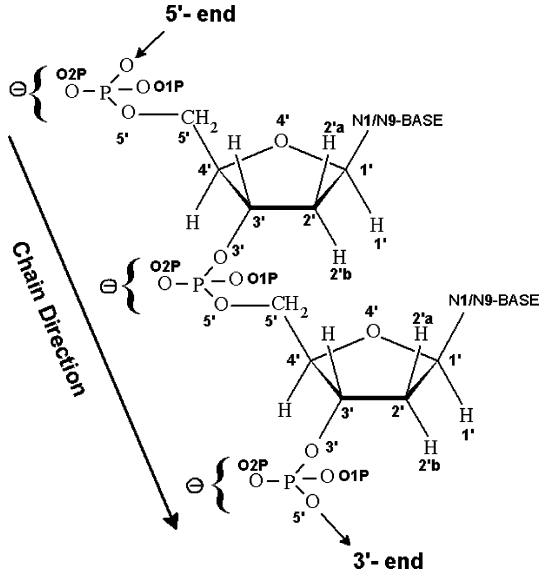

Figure 11. Numbering scheme of the backbone atoms in DNA.

own nucleotide (H1′). While the most significant interaction in this dinuclotide, this hydrogen bonding is, however, topologically unstable due to its proximity to its associated RCP. The next closed-shell interaction of significance is the one linking the backbone's O5′ of thymidine with H2′b of adenosine (ρ_b = 0.011). The latter atom, H2′b of adenosine, is involved in a trifurcated weak bonding arrangement with H6 and with O4′, both of thymidine, in addition to the already described hydrogen bonding to O5′ of thymidine. The adenosine sugar's H1′ is in its turn involved in a weak bifurcated hydrogen bond and hydrogen−hydrogen bond to O4′ and to H5′ of thymidine, ρ_b

= 0.005 and 0.003 au, respectively. Interestingly, adenine's N3 is bonded to thymidine's O4′ and simultaneously participates in a π-stacking interaction linking it to thymine's N1, both interactions exhibiting $\rho_b = 0.005$ au.

6. Conclusions

Several modes of bonding in nucleic acids are examined in this paper within the framework of AIM. These modes can be broadly classified as (1) WC hydrogen bonding between complementary bases on opposite strands of the α-helix, (2) π-stacking interactions between stacked successive base pairs, whether within a single strand of DNA (intrastrand) or crossing from one strand to the neighboring one (interstrand), (3) base−backbone interactions, and (4) backbone−backbone interactions.

A preliminary discussion of the relationship between the topological bond properties and the contribution of each bond within a WC base pair to the interaction energy is presented and will be completed in a subsequent publication. Base−base π-stacking is shown to be the reflection of several weak closed-shell bonding interactions linking the neighboring bases. Several other weak bonding interactions between the bases and the backbone atoms and between the backbone atoms and each other are also characterized topologically according to AIM.

The topological features described in this paper, while presented as a set of special-case studies of a sampling of experimental geometries, are expected to be ubiquitous to nucleic acid polymers. An infinite stack of DNA base pairs is a cylinder of electron density spanned along its length by a complex network of weak closed-shell interactions, each WC base pair being flanked by two zero-flux surfaces separating it from the two adjacent base pairs in the chain. The zero-flux surface lying between every neighboring base pair contains all the bond, ring, and cage critical points arising from their mutual interaction, namely, their π-stacking; see Figure 9.

Except for the relatively strong hydrogen bonding in the WC base pairs, most of the closed-shell interactions described in this paper are (very) weak. Collectively, however, these interactions are expected to influence nucleic acid geometry, stability, and reactivity. Fast and relatively accurate estimates of interaction energies from the topological properties at the BCP[58] or at the CCP between π-stacked rings[29] can be used in the future to estimate the contributions of π-stacking, base−backbone, and backbone−backbone to the stability of nucleic acids.

Acknowledgment. The authors acknowledge the Natural Sciences and Engineering Research Council of Canada (NSERC) for funding and the Killam Trusts for a Killam Postdoctoral Fellowship to C.F.M.

7. Appendix

7.1. Abbreviations. (1) Nucleobases: A = adenine, T = thymine, G = guanine, C = cytosine, and when confusion can arise, they are abbreviated Ade, Thy, Gua, and Cyt, respectively. The same abbreviations are also used to denote the corresponding nucleoside or nucleotide depending on the context.

(2) Backbone = BB and BB(X) denotes the backbone belonging to the nucleoside or nucleotide of base X.

(3) AIM = the quantum theory of atoms in molecules, BCP = bond critical point, RCP = ring critical point, CCP = cage critical point, bl = bond length (internuclear separation), bpl = bond path length (the length of the line of maximal electron density linking the nuclei of two bonded atoms), au = atomic units, WC = Watson and Crick.

(4) BSSE = basis set superposition error.

7.2. Definitions. In this paper, a **monomer** could be any one of the four DNA bases, A, G, C, or T. A **dimer** means a Watson−Crick hydrogen bonded dimer of complementary bases, that is, either A≡T or G≡C (these will be referred to as AT and GC, respectively, for simplicity). A **duplex** is a π-stacked system which could be either two π-stacked monomers (a duplex of monomers) or two π-stacked dimers (a duplex of dimers). An **intrastrand** stacking interaction is a weak bonding interaction linking two bases belonging to the same strand of the double helix in a duplex of dimers. An **interstrand** stacking interaction is a weak bonding interaction linking two bases belonging to the opposite strands of the double helix in a duplex of dimers. A **dinucleotide** is a monomer duplex, each with its deoxyribose sugar and phosphate moieties (its complete backbone), however, in the context of this paper, the term is synonymous to a 5′-pseudo-nucleotide-3′-nucleoside sequence, which is the truncated model we use for a dinucleotide (see the Results and Discussion section for details).

References and Notes

(1) Watson, J. D. *The Double Helix: A Personal Account of the Discovery of the Structure of DNA*; Stent, G. S., Ed.; W. W. Norton & Co.: New York, 1980.
(2) Watson, J. D.; Crick, F. H. C. *Nature* **1953**, *171*, 964−967.
(3) Watson, J. D.; Crick, F. H. C. *Nature* **1953**, *171*, 737−738.
(4) Watson, J. D.; Crick, F. H. C. *Cold Spring Harbor Symposia on Quantitative Biology*, *XVIII*; Cold Spring Harbor, NY, 1953; p 123−131.
(5) Crick, F. H. C.; Watson, J. D. *Proc. R. Soc. London, Ser. A* **1954**, *223*, 80−96.
(6) Wilkins, M. H. F.; Stokes, A. R.; Wilson, H. R. *Nature* **1953**, *171*, 738−740.
(7) Franklin, R. E.; Gosling, R. G. *Nature* **1953**, *171*, 740−741.
(8) Dickerson, R. E. DNA Structures: Part A, Synthesis and Physical Analysis of DNA. In *Methods in Enzymology*; Lilley, D. M. J., Dahlberg, J. E., Eds.; Academic Press: San Diego, CA, 1992; Vol. 211, p 67.
(9) Saenger, W. *Principles of Nucleic Acid Structure*; Springer-Verlag: New York, 1984.
(10) Sinden, R. R. *DNA Structure and Function*; Academic Press: San Diego, CA, 1994.
(11) Schlick, T. *Molecular Modeling and Simulation: An Interdisciplinary Guide*; Springer: New York, 2002.
(12) Bader, R. F. W. *Atoms in Molecules: A Quantum Theory*; Oxford University Press: Oxford, U.K., 1990.
(13) Mao, L.; Wang, Y.; Liu, Y.; Hu, X. *J. Mol. Biol.* **2004**, *336*, 787−807.
(14) Desfrançois, C.; Carles, S.; Schermann, J. P. *Chem. Rev.* **2000**, *100*, 3943−3962.
(15) Gorin, A. A.; Zhurkin, V. B.; Olson, W. K. *J. Mol. Biol.* **1995**, *247*, 34−48.
(16) Olson, W. K.; Gorin, A. A.; Lu, X.-J.; Hock, L. M.; Zhurkin, V. B. *Proc. Natl. Acad. Sci. U.S.A.* **1998**, *95*, 11163−11168.
(17) Gromiha, M. M. *J. Biotechnol.* **2005**, *117*, 137−145.
(18) Zhang, L.; Peritz, A.; Meggers, E. *J. Am. Chem. Soc.* **2005**, *127*.
(19) Mignon, P.; Loverix, S.; Steyaert, J.; Geerlings, P. *Nucleic Acid Res.* **2005**, *33*, 1779−1789.
(20) Hobza, P.; Šponer, J. *J. Am. Chem. Soc.* **2002**, *124*, 11802−11808.
(21) Sponer, J.; Berger, I.; Spackova, N.; Leszczynski, J.; Hobza, P. *J. Biomol. Struct. Dyn.* **2000**, *S2*, 383−407.
(22) Sponer, J.; Leszczynski, J.; Hobza, P. *J. Biomol. Struct. Dyn.* **1996**, *14*, 117−135.
(23) Oostenbrink, C.; van Gunsteren, W. F. *Chem.−Eur. J.* **2005**, *11*, 4340−4348.
(24) Delcourt, S. G.; Blake, R. D. *J. Biol. Chem.* **1991**, *266*, 15160−15169.
(25) Tsuzuki, S.; Uchimaru, T.; Mikami, M.; Tanabe, K. *Chem. Phys. Lett.* **1996**, *252*, 206−210.
(26) Ye, X.; Li, Z.-H.; Wang, W.; Fan, K.; Xu, W.; Hua, Z. *Chem. Phys. Lett.* **2004**, *397*, 56−61.
(27) Zhao, Y.; Truhlar, D. G. *J. Phys. Chem. A* **2005**, *109*, 4209−4212.
(28) Zhao, Y.; Truhlar, D. G. *J. Phys. Chem. A* **2005**, *109*, 5656−5667.
(29) Zhikol, O. A.; Shishkin, O.; Lyssenko, K. A.; Leszczynski, J. *J. Chem. Phys.* **2005**, *122*, 144104-1−144104-8.
(30) Bader, R. F. W. *Chem. Rev.* **1991**, *91*, 893−928.
(31) Bader, R. F. W. *Can. J. Chem.* **1998**, *76*, 973−988.
(32) Bader, R. F. W. In *Encyclopedia of Computational Chemistry*; Schleyer, P. v.-R., Ed.; John Wiley and Sons: Chichester, U.K., 1998; p 64.

(33) Bader, R. F. W. *Monatsh. Chem.* **2005**, *136*, 819−854.
(34) Popelier, P. L. A. *Atoms in Molecules: An Introduction*; Prentice Hall: London, 2000.
(35) Matta, C. F.; Gillespie, R. J. *J. Chem. Educ.* **2002**, *79*, 1141−1152.
(36) Bader, R. F. W. *J. Phys. Chem. A* **1998**, *102*, 7314−7323.
(37) Castillo, N.; Matta, C. F.; Boyd, R. J. *Chem. Phys. Lett.* **2005**, *409*, 265−269.
(38) Feigon, J.; Sklenár, V.; Wang, E.; Gilbert, D. E.; Macaya, R. F.; Schultze, P. DNA Structures, Part A−Synthesis and Physical Analysis of DNA. In *Methods in Enzymology*; Lilley, D. M. J.; Dahlberg, J. E., Eds.; Academic Press: New York, 1992; Vol. 211, p 235.
(39) Feigon, J.; Wang, A. H. J.; van der Marel, G. A.; Van Boom, J. H.; Rich, A. *Nucleic Acids Res.* **1984**, *12*, 1243−1263.
(40) Gilbert, D. E.; Feigon, J. *Biochemistry* **1991**, *30*, 2483−2494.
(41) Evans, F. E.; Kaplan, N. O. *J. Biol. Chem.* **1976**, *251*, 6791−6797.
(42) Hocquet, A.; Ghomi, M. *Phys. Chem. Chem. Phys.* **2000**, *2*, 5351−5353.
(43) Hocquet, A. *Phys. Chem. Chem. Phys.* **2001**, *3*, 3192−3199.
(44) Louit, G.; Hocquet, A.; Ghomi, M. *Phys. Chem. Chem. Phys.* **2002**, *4*, 3843−3848.
(45) Sujatha, M. S.; Sasidhar, Y. U.; Balaji, P. V. *Biochemistry* **2005**, *44*, 8554−8562.
(46) Fernández-Alonso, M. C.; Cañada, F. J.; Jiménez-Barbero, J.; Cuevas, G. *J. Am. Chem. Soc.* **2005**, *127*, 7379−7386.
(47) Dornberger, U.; Flemming, J.; Fritzsche, H. *J. Mol. Biol.* **1998**, *284*, 1453−1463.
(48) Shui, X.; Sines, C. S.; McFail-Isom, L.; VanDerveer, D.; Williams, L. D. *Biochemistry* **1998**, *37*, 16877−16887.
(49) Shui, X.; McFail-Isom, L.; Hu, G. G.; Williams, L. D. *Biochemistry* **1998**, *37*, 8341−8355.
(50) Frisch, M. J.; Trucks, G. W.; Schlegel, H. B.; Scuseria, G. E.; Robb, M. A.; Cheeseman, J. R.; Montgomery, J. A., Jr.; Vreven, T.; Kudin, K. N.; Burant, J. C.; Millam, J. M.; Iyengar, S. S.; Tomasi, J.; Barone, V.; Mennucci, B.; Cossi, M.; Scalmani, G.; Rega, N.; Petersson, G. A.; Nakatsuji, H.; Hada, M.; Ehara, M.; Toyota, K.; Fukuda, R.; Hasegawa, J.; Ishida, M.; Nakajima, T.; Honda, Y.; Kitao, O.; Nakai, H.; Klene, M.; Li, X.; Knox, J. E.; Hratchian, H. P.; Cross, J. B.; Adamo, C.; Jaramillo, J.; Gomperts, R.; Stratmann, R. E.; Yazyev, O.; Austin, A. J.; Cammi, R.; Pomelli, C.; Ochterski, J. W.; Ayala, P. Y.; Morokuma, K.; Voth, G. A.; Salvador, P.; Dannenberg, J. J.; Zakrzewski, V. G.; Dapprich, S.; Daniels, A. D.; Strain, M. C.; Farkas, O.; Malick, D. K.; Rabuck, A. D.; Raghavachari, K.; Foresman, J. B.; Ortiz, J. V.; Cui, Q.; Baboul, A. G.; Clifford, S.; Cioslowski, J.; Stefanov, B. B.; Liu, G.; Liashenko, A.; Piskorz, P.; Komaromi, I.; Martin, R. L.; Fox, D. J.; Keith, T.; Al-Laham, M. A.; Peng, C. Y.; Nanayakkara, A.; Challacombe, M.; W. Gill, P. M.; Johnson, B.; Chen, W.; Wong, M. W.; Gonzalez, C.; Pople, J. A. *Gaussian03, Revision B.03*; Gaussian Inc.: Pittsburgh, PA, 2003.
(51) Biegler-König, F. W.; Schönbohm, J.; Bayles, D. *J. Comput. Chem.* **2001**, *22*, 545−559.
(52) Crick, F. H. C. *J. Mol. Biol.* **1966**, 548−555.
(53) Leonard, G. A.; McAuley-Hecht, K.; Brown, T.; Hunter, W. N. *Acta Crystallogr. D* **1995**, *51*, 136−139.
(54) Parthasarathi, R.; Amutha, R.; Subramanian, V.; Nair, B. U.; Ramasami, T. *J. Phys. Chem. A* **2004**, *108*, 3817−3828.
(55) Asensio, A.; Kobko, N.; Dannenberg, J. J. *J. Phys. Chem. A* **2003**, *107*, 6441−6443.
(56) Boyd, R. J.; Choi, S. C. *Chem. Phys. Lett.* **1986**, *129*, 62−65.
(57) Carroll, M. T.; Bader, R. F. W. *Mol. Phys.* **1988**, *65*, 695−722.
(58) Espinosa, E.; Molins, E.; Lecomte, C. *Chem. Phys. Lett.* **1998**, *285*, 170−173.
(59) Grabowski, S. J. *J. Phys. Chem. A* **2001**, *105*, 10739−10746.
(60) Domagala, M.; Grabowski, S.; Urbaniak, K.; Mloston, G. *J. Phys. Chem. A* **2003**, *107*, 2730−2736.
(61) Grabowski, S.; Sokalski, W. A.; Leszczynski, J. *J. Phys. Chem. A* **2005**, *109*, 4331−4341.
(62) Domagala, M.; Grabowski, S. *J. Phys. Chem. A* **2005**, *109*, 5683−5688.
(63) Espinosa, E.; Molins, E. *J. Chem. Phys.* **2000**, *113*, 5686−5694.
(64) Bader, R. F. W. *Phys. Rev. B* **1994**, *49*, 13348−13356.
(65) Cremer, D.; Kraka, E. *Angew. Chem., Int. Ed. Engl.* **1984**, *23*, 627−628.
(66) Matta, C. F.; Boyd, R. J., to be submitted.
(67) Knop, O.; Rankin, K. N.; Boyd, R. J. *J. Phys. Chem. A* **2001**, *105*, 6552−6566.
(68) Matta, C. F.; Hernández-Trujillo, J.; Tang, T. H.; Bader, R. F. W. *Chem.−Eur. J.* **2003**, *9*, 1940−1951.
(69) Robertson, K. N.; Knop, O.; Cameron, T. S. *Can. J. Chem.* **2003**, *81*, 727−743.
(70) Matta, C. F. In *Hydrogen Bonding−New Insight, (Challenges and Advances in Computational Chemistry and Physics Series)*; Grabowski, S., Ed.; Kluer: 2006.
(71) Popelier, P. L. A. *J. Phys. Chem. A* **1998**, *102*, 1873−1878.
(72) Bone, R. G. A.; Bader, R. F. W. *J. Phys. Chem.* **1996**, *100*, 10892−10911.
(73) Gibbs, G. V.; Boisen, M. B., Jr.; Rosso, K. M.; Teter, D. M.; Bukowinski, M. S. T. *J. Phys. Chem. B* **2000**, *104*, 10534−10542.
(74) Bianchi, R.; Gervasio, G.; Marabello, D. *Inorg. Chem.* **2000**, *39*, 2360−2366.
(75) Zhurova, E. A.; Tsirelson, V. G.; Stash, A. I.; Pinkerton, A. A. *J. Am. Chem. Soc.* **2002**, *124*, 4574−4575.
(76) Boisen, M. Private communication, 2005.
(77) Platts, J. A.; Howard, S. T.; Fallis, I. A. *Chem. Phys. Lett.* **1998**, *285*, 198−204.
(78) Matta, C. F.; Castillo, N.; Boyd, R. J. *J. Phys. Chem. A* **2005**, *109*, 3669−3681.